remote sensing

MDPI

Article

Spatiotemporal Dynamic Changes in Cropland and Multi-Scenario Simulation in the Yarlung Zangbo River Basin

Mengni He [1], Yanguo Liu [1,*], Liwei Tan [1], Jingji Li [2], Ziqin Wang [2], Yafeng Lu [3], Wenxu Liu [1] and Qi Tan [1]

[1] Mianyang Science and Technology City Division, the National Remote Sensing Center of China, Southwest University of Science and Technology, Mianyang 621010, China; 13649062214@163.com (M.H.); 18081538425@163.com (L.T.); 13882773715@163.com (W.L.); 19961108546@163.com (Q.T.)
[2] State Key Laboratory of Geo-Hazard Prevention and Geo-Environment Protection, Chengdu University of Technology, Chengdu 610059, China; lijingji2014@cdut.edu.cn (J.L.); 18239769691@163.com (Z.W.)
[3] Institute of Mountain Hazards and Environment, Chinese Academy of Sciences, Chengdu 610041, China; luyafeng@imde.ac.cn
* Correspondence: liuyg2008@126.com

Abstract

Cropland is crucial for food production, food security, and economic stability, especially in high-altitude Tibetan regions where it is limited. This study investigates the spatiotemporal changes and driving factors of cropland in the Yarlung Zangbo River Basin (YZRB) from 2000 to 2020. Using land use transfer matrices, center of gravity models, standard deviation ellipses, the Patch-generating Land Use Simulation (PLUS) model, and Partial Least Squares Structural Equation Modeling (PLS-SEM), it explores cropland dynamics and predicts land use for 2030. Results show the following: (1) Between 2000 and 2020, the area of cropland entering the basin exceeded that leaving, mainly concentrated in the middle and lower reaches, with a dynamic degree of 0.97%. The proportion of cropland increased from 1.28% in 2000 to 1.52% in 2020. (2) The center of gravity shifted northwest (2000–2005), southeast (2005–2015), and northwest again (2015–2020). (3) Factors like elevation, temperature, precipitation, population density, and GDP correlated with cropland changes. Natural factors positively affected cropland expansion, while socioeconomic and proximity factors indirectly inhibited it. (4) The 2030 cropland conservation scenario in the PLUS model ensures cropland security, ecological protection, and controlled construction land expansion, aligning with the Sustainable Development Goals. Targeted cropland conservation measures can effectively promote sustainable land use and ecological security in the Yarlung Zangbo River Basin.

Keywords: cropland; spatiotemporal evolution; PLUS model; PLS-SEM model; Yarlung Zangbo River Basin

check for updates

Academic Editor: Xihua Yang

Received: 20 May 2025
Revised: 27 June 2025
Accepted: 3 July 2025
Published: 7 July 2025

Citation: He, M.; Liu, Y.; Tan, L.; Li, J.; Wang, Z.; Lu, Y.; Liu, W.; Tan, Q. Spatiotemporal Dynamic Changes in Cropland and Multi-Scenario Simulation in the Yarlung Zangbo River Basin. *Remote Sens.* **2025**, *17*, 2328. https://doi.org/10.3390/rs17132328

Copyright: © 2025 by the authors. Licensee MDPI, Basel, Switzerland. This article is an open access article distributed under the terms and conditions of the Creative Commons Attribution (CC BY) license (https://creativecommons.org/licenses/by/4.0/).

1. Introduction

Cropland, as the foundation of national food security and socio-ecological sustainability, has long been a focal point of scientific and policy discourse [1,2]. In the context of ongoing global population growth, decreasing per capita cropland, and significant challenges to food security, the systematic mapping of the global cropland distribution patterns and the accurate understanding of their spatiotemporal patterns of change are of critical importance for food security governance [3–5]. Nowadays, cropland resources are facing dual challenges of area contraction and quality deterioration, particularly pronounced in ecologically vulnerable regions [6,7]. Research on cropland dynamics has

evolved from single–factor analysis to multi-dimensional coupling mechanisms. At the global scale, extreme climate events have imposed significant stress on cropland systems. For instance, compound drought and heatwave events (CDHEs) are projected to multiply global cropland exposure risks in the mid to late 21st century, with climate change being the dominant driver [8]. In China, cropland dynamics exhibit pronounced regional differentiation. Cropland has expanded in arid and semi-arid areas west of the Hu Line and on the Qinghai-Tibetan Plateau, while shrinking in eastern coastal and economically developed regions due to urban encroachment. This process is jointly driven by natural factors (e.g., elevation, precipitation) and socioeconomic factors (e.g., population density, agricultural mechanization) [9,10]. Research on high-altitude croplands has primarily focused on the Qinghai-Tibetan Plateau and the Loess Plateau. Niche–based research indicates that cropland transitions in agro-pastoral areas are largely shaped by grassland niche shifts and driven by social interests [11,12]. During the grassland–cropland–shrubland conversion, soil microbial network complexity has shown greater predictive power for ecosystem multifunctionality than microbial diversity, with soil phosphorus identified as a key regulatory factor [12]. Additionally, recent studies have systematically mapped the environmental impacts of cropland abandonment in mountainous areas, revealing research themes, spatial distributions, methodological gaps, and knowledge deficiencies [13]. However, current research remains largely centered on biodiversity and soil processes, with limited attention to the spatiotemporal drivers and multi-scenario simulations of cropland dynamics in high-altitude basins.

In recent years, the rapid development of remote sensing technology and Geographic Information Systems (GIS) has provided unprecedented technical support for large-scale, long-term land use change analyses [14–16]. However, traditional models still exhibit limitations in simulating cropland dynamics in high-altitude regions. For example, the CA-Markov model [17,18] relies on a static transition probability matrix, making it incapable of capturing the effects of dynamic factors such as climate warming and policy adjustments on land use transitions. Moreover, it typically applies fixed neighborhood windows (e.g., 3×3 or 5×5), which fail to account for terrain—induced barriers to spatial interactions, such as mountainous areas that constrain the potential expansion of cropland. While the CLUE–S model [19,20] incorporates macro-level driving factors, it shows limited capacity in capturing micro-scale spatial heterogeneity, such as the patchy and fragmented distribution of cropland in valley regions. The FLUS model [21,22] achieves higher accuracy than the aforementioned models; however, its suitability surface is derived from logistic regression, which may overlook localized ecological constraints in areas with complex topography. These models tend to produce inconsistent simulation accuracies across different land use types. In contrast, the PLUS model demonstrates more accurate performance in land use simulation, offering significant advantages in both spatial representation and quantitative reliability, particularly under conditions of high landscape heterogeneity [20]. For example, Zhang et al. [23] combined Random Forest (RF), Support Vector Machine (SVM), and Artificial Neural Network (ANN) algorithms to analyze land use changes in the Southwest Guangxi Karst-Beibu Gulf region (1990–2020), subsequently projecting ecological carrying capacity (2030–2040) via the PLUS model. Zhang et al. [24] coupled the PLUS model (land use simulation) with the InVEST model (carbon stock assessment) to quantify scenario–based carbon dynamics in Hohhot (2000–2030). Concurrently, the PLS-SEM model has made significant advances in analyzing complex variable relationships. For instance, the PLS-SEM model has advanced the analysis of latent variables in wetland studies, effectively resolving nonlinear interactions among natural and socioeconomic drivers [25]. Wang et al. [26] elucidated composite effects of topography, urbanization, and climate change on

wetland distribution in Wuhan through PLS-SEM, identifying indirect regulatory pathways among variables.

Research on the Yarlung Zangbo River Basin has primarily focused on land cover classification [27], basin-scale environmental transitions [28], and hydrological-ecological interactions [29,30]. However, existing studies lack a mechanistic exploration of cropland dynamics, particularly in multi-scenario forecasting and process-based driving force analysis. Current research disproportionately focuses on major grain-producing regions (e.g., Northeast Plain, North China Plain), with limited attention to alpine watershed agroecosystems [31–33].

The Yarlung Zangbo River Basin (YZRB), located in the core area of the Tibetan Plateau, functions as both an essential ecological barrier and an agro-pastoral transition zone in China. Cropland within this basin represents a strategically vital yet ecologically constrained resource, critical for socioeconomic stability on the plateau. Despite its area accounting for only approximately 1% of the total land area of the plateau [34], it faces compounding pressures from intensifying land use and conservation trade-offs. The middle reaches of the YZRB, characterized by high solar irradiance, irrigation infrastructure density, and elevated population density, are recognized as "Tibet's granary". This region sustains 50.56% of Tibet's cropland and serves as the primary production hub for highland barley. Its cropland dynamics directly mediate plateau-scale grain self-sufficiency, thereby influencing socio-ecological resilience and sustainable development trajectories in this fragile alpine system.

To address these challenges, spatial dynamics are analyzed through centroid migration modeling and standard deviational ellipse (SDE) to delineate directional shifts in cropland distribution. The PLUS model projects 2030 land use configurations under four policy scenarios: natural development scenario (NDS), cropland protection scenario (CPS), ecological protection scenario (EPS), and Urban development scenario (UDS). The PLS-SEM model decouples the multi-scale interactions among natural drivers (temperature, precipitation, topography), socioeconomic variables (population, GDP), and accessibility factors (road network proximity), elucidating hierarchical causation mechanisms. These integrated approaches collectively inform adaptive land management strategies to balance grain security imperatives with alpine ecosystem integrity, providing scenario–based decision frameworks for the YZRB's sustainable development. The methodology establishes a transferable paradigm for managing cropland in comparable fragile ecoregions. The overall research framework is shown in Figure 1.

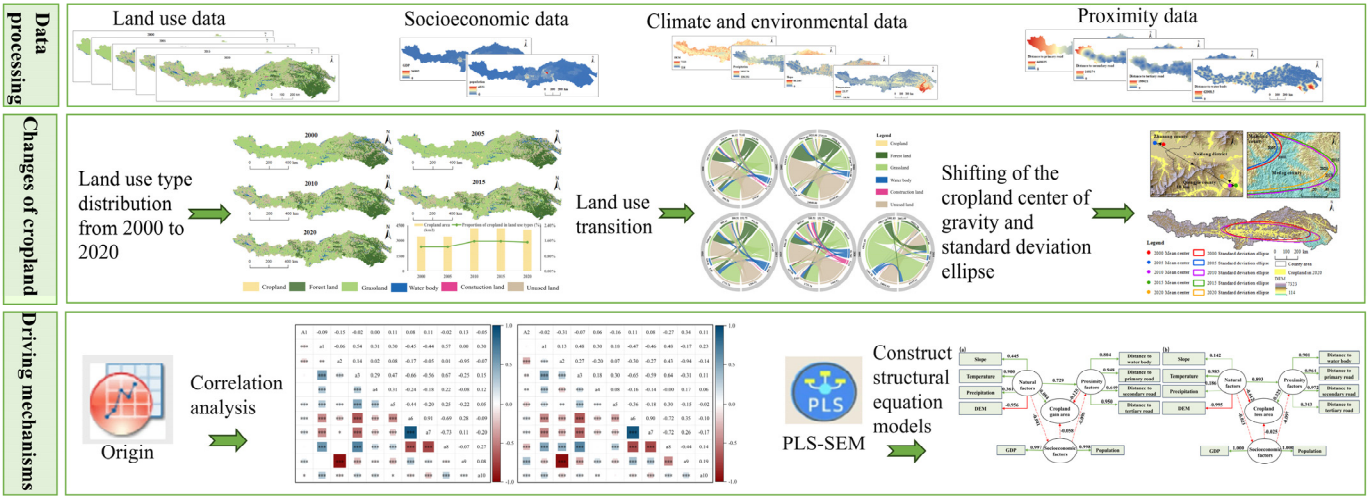


Figure 1. *Cont.*

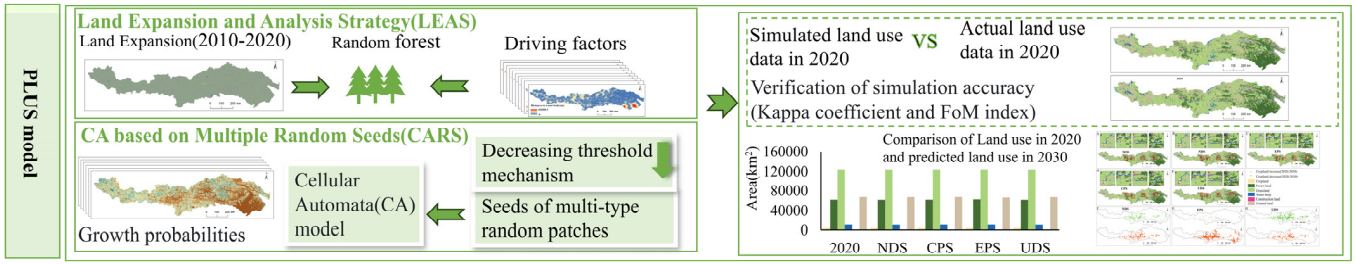


Figure 1. The framework of the study.

2. Materials and Methods

2.1. Study Area

The Yarlung Zangbo River Basin (YZRB), situated in the southeastern Tibetan Plateau (27.81°N–31.28°N, 82.01°E–97.10°E), is bounded by the Gangdise-Nianqing Mountains Range to the north and the Himalayas to the south, forming a pivotal component of Asia's Water Tower (Figure 2). Originating from the Jiemayangzong Glacier (5590 m asl) on the Himalayas' northern slope, the river traverses seven prefecture-level cities (Ali, Rikaze, Naqu, Shannan, Lasa, Linzhi, Changdu) across the Tibet Autonomous Region (TAR), spanning 2057 km in length with a drainage area of 270,500 km^2. Characterized by extreme elevational gradients (115–7294 m asl), it represents the world's highest-altitude fluvial system (mean elevation > 4500 m).

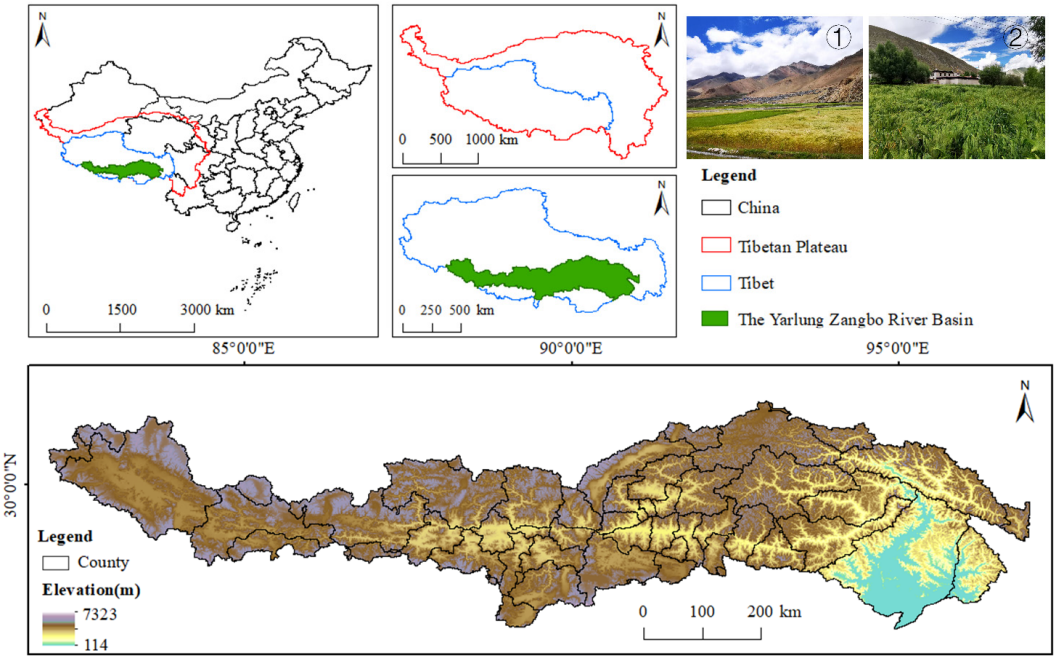


Figure 2. Location of the study area (the background image shows the cropland in the Yarlung Zangbo River Basin, taken by Yanguo Liu during fieldwork. Both Figure ① and ② show highland barley. Figure ① was taken in Lazi County, Rikaze City on 10 August 2023; Figure ② was taken in Nimu County, Lasa City on 23 August 2023.

Climatic heterogeneity across elevational zones manifests as west–east transitions from semi-arid to subtropical humid regimes, with pronounced monsoonal seasonality. The upper basin exhibits alpine frigid semi-arid conditions (mean annual temperature: 0–3 °C; precipitation < 300 mm/yr), transitioning to temperate semi-arid zones in mid-reaches (5–9 °C; 300–600 mm/yr), and subtropical montane humid climates in lower reaches (precipitation 600–800 mm/yr). Hydrologically, the system derives 1.65 × 10^{11} m^3 annual

discharge primarily from precipitation (78% contribution), supplemented by cryospheric meltwater (15%) and groundwater (7%), yielding 139.5 km^3/yr total runoff. Despite occupying 22.5% of TAR's territory, the YZRB sustains > 50% of TAR's population (mid-lower reach concentration) and 75% of regional GDP. Its 3163.85 km^2 cropland (71.57% of TAR's total) constitutes Tibet's agroecological core, specializing in highland barley (*Hordeum vulgare* L.), rapeseed (*Brassica napus*), and legumes (*Fabaceae* spp.), which collectively account for 82% of regional staple crop yields.

2.2. Data Sources

A summary of the data description is shown in Table 1. All datasets were resampled to 30-m spatial resolution and temporally harmonized to 2020 through nearest-neighbor interpolation. WGS 1984 Albers Equal Area Conic projection was applied to ensure pixel-to-pixel alignment across socioeconomic, bioclimatic, and transportation accessibility raster layers. Figure 3 illustrates the primary driving factors.

Table 1. The spatial driving factors of the land use change.

Type	Data	Data Sources	Original Resolution	Year
Land use data	Land use classification data of the study area	Resource and Environmental Science and Data Center, Chinese Academy of Sciences (https://www.resdc.cn) (accessed on 14 August 2024)	30 m	2000, 2005, 2010, 2015, and 2020
	Permanent basic farmland Ecological red line Nature reserve	The Department of Natural Resources of the Tibet Autonomous Region (accessed on 13 April 2025)		
Socioeconomic data	Population GDP	Resource and Environmental Science and Data Center, Chinese Academy of Sciences (https://www.resdc.cn) (accessed on 13 September 2024)	1000 m	2020
Climate and environmental data	Temperature Precipitation			
	DEM Slope	Geospatial Data Cloud (accessed on 13 September 2024)	30 m	
	Distance to water body	OpenStreetMap (https://www.openstreetmap.org/) (accessed on 13 September 2024)		
Proximity data	Distance to primary road Distance to secondary road Distance to tertiary road	Resource and Environmental Science and Data Center, Chinese Academy of Sciences (https://www.resdc.cn) (accessed on 14 August 2024)	1000 m	

2.3. Methods

2.3.1. Land Use Transition Matrix

The land use transition matrix is a dynamic analysis method for changes in land use patterns. Through the land use transition matrix, the mutual conversion of different land use types between two periods can be effectively reflected. It can describe the structural characteristics of land use changes and highlight the direction of change in different land categories at the beginning and end of a period in a particular region, while better illustrating the spatiotemporal evolution process of land use types [35].

Using ArcGIS 10.8 software, overlay analysis of land use maps from 2000 to 2020 can yield the land use transition matrix for different periods in the study area, which helps in analyzing the conversion between land use types. The general formula for this is as follows:

$$S_{ij} = \begin{bmatrix} S_{11} & S_{12} & \cdots & S_{1n} \\ S_{21} & S_{22} & \cdots & S_{2n} \\ \vdots & & \ddots & \vdots \\ S_{n1} & S_{n2} & \cdots & S_{nn} \end{bmatrix} \quad (1)$$

where S represents the area in km^2; n denotes the number of land use types before and after the transition; i and j refer to the land use types before and after the transition, respectively; and S_{ij} is the area in km^2 of land type i transitioning to land type j.

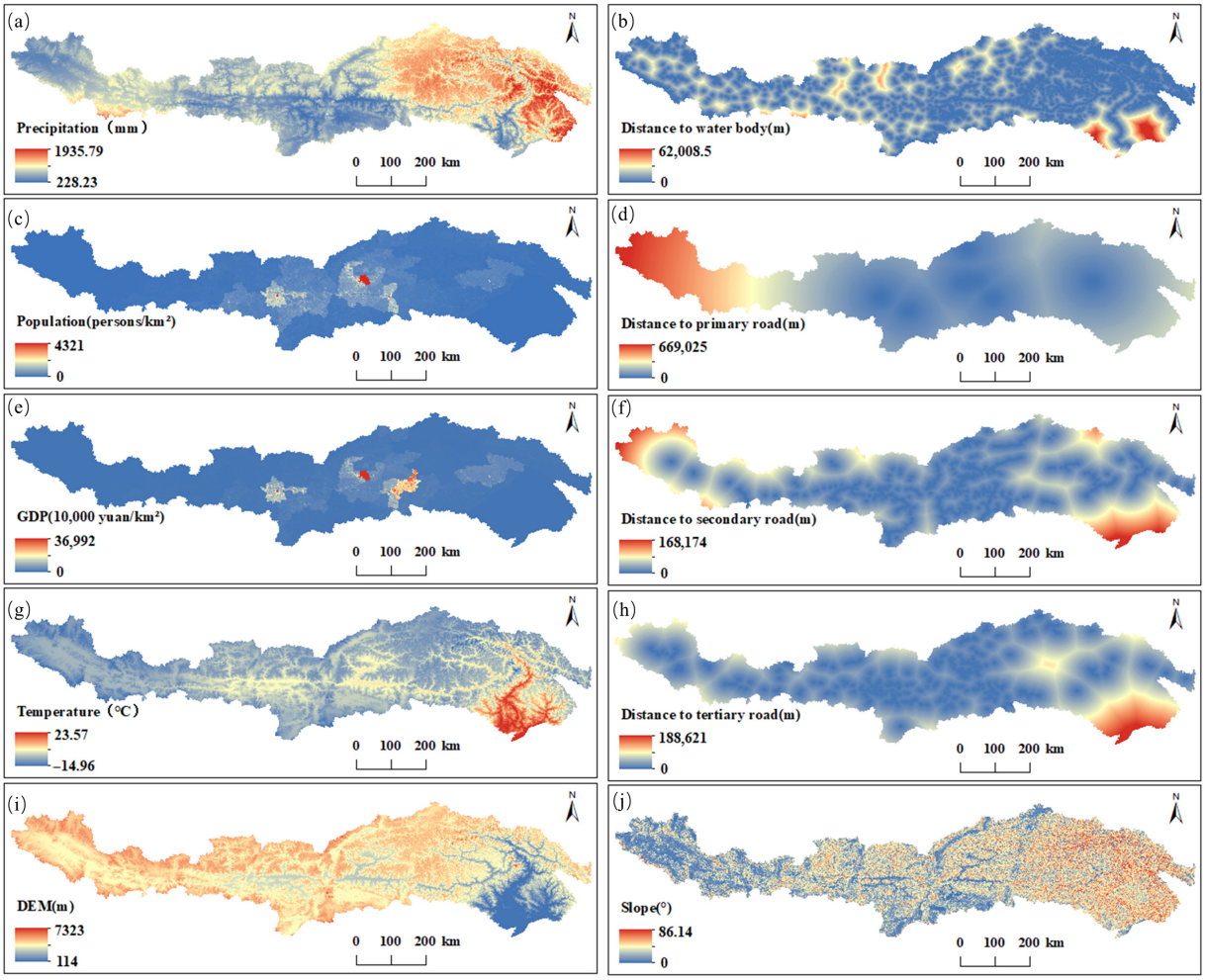


Figure 3. Driving factors of land use change. (Subfigure (**a**–**j**) represent the driving factors:precipitaition, distance to water body, population, distance to primary road, GDP, distance to secondary road, temperature, distance to tertiary road, DEM, and slope).

2.3.2. Land Use Dynamic Degree

The Single Land Use Dynamic Degree (SLUDD) represents the degree and rate of area change in a specific land use type within a designated area over a specific period [36]. It provides an intuitive measure of the scale and speed of land use changes. SLUDD quantifies the spatiotemporal change rate of specific land use types in the study area [37]. Therefore, the analysis of the rate of cropland use change in the study area can be conducted using this model, as expressed in the following formula:

$$K = (U_b - U_a)/U_a \times (1/T) \times 100\% \quad (2)$$

where U_a represents the area of cropland at the beginning of the study period for the research unit; U_b indicates the area of cropland at the end of the study period; T denotes the duration of the study period; and K represents the dynamic degree of cropland during period T (i.e., the rate of cropland change).

2.3.3. Center of Gravity Model

The center of gravity model originates from the concept of "center of gravity" in physics, referring to the point at which the resultant force of gravity acts upon a body. This concept has been extended to various disciplines and is widely applied in spatial sciences to analyze spatial distribution patterns, dynamic evolution, and system cores. In the context of geographic research, the model provides an effective approach for quantifying spatial displacement and detecting structural changes associated with regional development drivers [38–40].The direction, distance, and speed of the migration of the centroid of each land use type are analyzed to reflect the spatial change trends, mobility, and spatial aggregation of land use in the region. The direction of centroid migration and transfer distance can be expressed through changes in the centroid coordinates [41]. The calculation of the regional centroid coordinates is shown in formulas (3) and (4):

$$X = \sum_{i=1}^{n} C_i X_i / \sum_{i}^{n} C_i \quad (3)$$

$$Y = \sum_{i=1}^{n} C_i y_i / \sum_{i}^{n} C_i \quad (4)$$

where X and Y represent the longitude and latitude of the centroid of a specific study attribute, respectively; X_i and Y_i denote the coordinates of region i, and C_i represents region i.

2.3.4. Standard Deviation Ellipse

The standard deviation ellipse method is a statistical approach used to analyze the spatial relationships of geographic features. It is employed to measure the direction and distribution within a given spatial area [42]. The long and short axes of the ellipse represent the direction and extent of cropland distribution, respectively. The ratio of the axes, known as the flatness ratio, indicates the directionality of the distribution; a larger ratio suggests stronger directionality. Weaker directionality and a broader value gap result in a smaller ratio, approaching a circular shape [43,44]. The standard deviation ellipse effectively reveals the overall characteristics and migration trends of cropland spatial distribution in the YZRB.

2.3.5. PLS-SEM

In order to analyze the factors influencing the change in cropland area, this study employs a structural equation model (SEM) with multiple influencing variables as the analytical framework. Partial Least Squares Structural Equation Modeling (PLS-SEM) is a multivariate statistical method used to study complex causal relationships. Unlike other methods, it does not require a large sample size, allowing a minimum sample size of 20 [45]. PLS-SEM is particularly advantageous in handling multicollinearity between variables, as it uses weights and loadings to minimize shared variance while maximizing predictive accuracy [46]. It integrates the characteristics of principal component analysis, multiple regression analysis, and path analysis. Compared to traditional covariance–based structural equation modeling (CB-SEM), PLS-SEM does not require strict assumptions about data distribution or normality, making it better suited for handling non-normal data often encountered in empirical research [47]. The PLS-SEM model consists of two main components: the measurement model, which describes the relationship between latent and observed variables, and the structural model, which describes the relationships between latent variables. The parameter estimation of PLS-SEM involves two steps: first, estimating the latent variable scores through iterative calculations; second, applying partial least squares regression to estimate the parameters of the structural and measurement models.

Assuming there are k latent variables, each corresponding to a set of m observed variables, the observed variables for each set can be represented as follows:

$$X_i = \{x_{i1},\ x_{i2},\ x_{i3}, \ldots,\ x_{im}\}, i\ =\ [1,2,3 \ldots k] \tag{5}$$

At the same time, it is assumed that there is a linear combination relationship between latent variables and between latent and observed variables, with each observed variable being associated with a unique latent variable. Therefore, the equation for the measurement model is as follows:

$$x_{ij} = \{\lambda_{ij}\xi_i + \sigma_{ij}\}(i\ = 1,2,3, \ldots,\ k;\ j =\ 1,\ 2,\ 3 \ldots,\ m_i) \tag{6}$$

$$\xi_i = \sum_{i \neq j} \beta_{ij}\xi_j + \varepsilon_i \tag{7}$$

where ξ_i represents the standardized latent variable, λ_{ij} denotes the factor loading, β_{ij} is the path coefficient, σ_{ij} and ε_i are error terms, which are uncorrelated with the predictor variables and have a mean of zero.

In this study, the latent variables include natural factors, socio-economic factors, and proximity factors. The observed variables consist of annual precipitation, annual average temperature, elevation, slope, population density, GDP, distance to primary/secondary/tertiary roads, and distance to a water body. The datasets of the ten driving factors were rasterized, and the average values of the driving factors were extracted from each grid at a resolution of 1 × 1 km to form the sample set.

2.3.6. PLUS Model

The PLUS model is a cellular automaton (CA) model based on raster data, designed for simulating land use/land cover (LULC) changes at the patch scale. The PLUS model integrates a rule-mining method based on land expansion analysis and a CA model based on a multi-type random seed mechanism. It can be used to identify the driving factors of land expansion and predict the patch-level evolution of land use landscapes [48]. The model first extracts the expansion portions of each land use type from the land change between two periods and uses the random forest algorithm to estimate the development probabilities of various land uses. It then employs a CA model with multi-type random patches to simulate future land use scenarios. Considering the reliability and scientific accuracy of the data, and taking into account the actual conditions of the study area, this study selects 10 driving factors, including elevation, slope, annual average temperature, annual precipitation, population, GDP, distance to primary/secondary/tertiary roads, and distance to water body, as the driving factors for land use change.

The parameters of this model were subject to relevant validation, including FoM, OA (overall accuracy), and Kappa coefficient [49]. Kappa is an index used to evaluate the accuracy of multi-class land use simulation and prediction. The results derived from the confusion matrix, which represents the overlay of the land use simulation results with the actual land use data, can be expressed as follows:

$$Kappa = (p_0 - p_c)/(p_p - p_c) \tag{8}$$

where P_o represents the proportion of correctly simulated instances, P_c is the expected proportion of correctly simulated instances under random conditions, and P_p refers to the proportion of correctly simulated instances in an ideal classification scenario. In the *Kappa* coefficient test, the value ranges from 0 to 1. The higher the *Kappa* coefficient, the greater the consistency between the model test results and the actual current state, thereby reflecting the higher accuracy of the simulated predictions. A *Kappa* coefficient greater than 0.75

indicates high consistency and prediction accuracy, a value between 0.40 and 0.75 indicates moderate consistency, and a value lower than 0.40 suggests poor consistency and lower prediction accuracy.

In the accuracy assessment of the PLUS model, the Kappa coefficient is commonly used as a measure of overall agreement; however, it has certain limitations. The F1-score serves as a complementary metric that addresses some of the shortcomings of Kappa by evaluating the balance between precision and recall. This makes it particularly suitable for scenarios with imbalanced samples or where detailed classification accuracy of specific categories is emphasized. The F1-score incorporates both the precision and recall of the classification model, functioning as a weighted harmonic mean of the two. Its value ranges from 0 to 1, with higher values indicating better model performance. Precision (P) refers to the proportion of correctly predicted positive samples (true positives) among all samples predicted as positive. Recall (R) refers to the proportion of correctly predicted positive samples (true positives) among all actual positive samples.

The formulas are defined as follows:

$$P = TP/(TP + FP),\ R = TP/(TP + FN) \tag{9}$$

$$F_1 = (2 \times P \times R)/(P + R) \tag{10}$$

where TP (True Positive) refers to the number of samples that are actually positive and correctly predicted as positive; FP (False Positive) refers to the number of samples that are actually negative but incorrectly predicted as positive; and FN (False Negative) refers to the number of samples that are actually positive but incorrectly predicted as negative.

FoM is a reliable metric for evaluating model performance in land use simulations. The parameter values derived from FoM can be used to assess whether the model can accurately simulate land use imagery and effectively measure the consistency between the changes in real and simulated imagery [50]. This coefficient is superior to the Kappa coefficient in evaluating the accuracy of simulated changes [21]. The equation is as follows:

$$FoM = B/(A + B + C + D) \tag{11}$$

where A represents the error area predicted as persistent due to observed changes, B represents the accurate area predicted as change due to observed changes, C represents the error area where observed changes are predicted as a switch to an incorrect category, and D represents the error area where observed persistence is predicted as change. The closer the FoM value is to 1, the higher the prediction accuracy in the change areas. Based on the land spatial development and protection goals outlined in the "Tibet Autonomous Region Land Spatial Planning (2021–2035)" and its vision for promoting ecological restoration, this study integrates these goals with the land type distribution of the study area. Therefore, four scenarios are formulated to simulate and evaluate the future spatiotemporal dynamics of various land use types.

(1) Natural development scenario (NDS): Based on the evolution of land types in the YZRB from 2000 to 2020, the Markov chain in the PLUS model is used to predict land use demand in the YZRB for 2030, without setting the probabilities of mutual conversion between land categories [51].

(2) Urban development scenario (UDS): The probability of conversion from cropland, forestland, grassland, and unused land to construction land is increased by 20%, while the probability of conversion from construction land to other land types, excluding cropland, is decreased by 30% [52].

(3) Ecological protection scenario (EPS): Except for construction land, all other land use categories are allowed to convert to forestland and grassland. To enhance ecological conservation, the probability of conversion from forestland and grassland to construction land was reduced by 50%, and that from cropland to construction land was reduced by 30%. Meanwhile, the probability of conversion from cropland and grassland to forestland increased by 30% [53]. Additionally, natural reserves and areas within ecological red lines were defined as restricted zones where land use transitions are not permitted.

(4) Cropland protection scenario (CPS): Cropland is the foundation for ensuring food supply and food security. The probability of conversion from forestland and grassland to construction land is reduced by 20%, and the probability of conversion from cropland to construction land is reduced by 60% [54,55]. Permanent basic cropland is set as a conversion–restricted zone.

The transformation cost matrix indicates the difficulty of transforming land type from the current to the demand. Only two values exist in the transformation cost matrix, 0 and 1. When the cost matrix value is 0, it indicates that the transformation of the land use class to another land use class is not allowed, and if it becomes 1, the opposite is true [56]. This study needs to form four transformation cost matrices corresponding to different scenarios (Table 2).

Table 2. Transition matrix of land use in different land simulation scenarios.

Land Use Type	NDS						CPS						EPS						UDS					
	a	**b**	**c**	**d**	**e**	**f**	**a**	**b**	**c**	**d**	**e**	**f**	**a**	**b**	**c**	**d**	**e**	**f**	**a**	**b**	**c**	**d**	**e**	**f**
a	1	0	1	0	1	1	1	0	0	0	0	0	1	1	1	1	1	1	1	0	0	0	1	1
b	0	1	1	0	0	1	1	1	1	0	0	1	0	1	0	0	0	0	1	1	0	0	1	1
c	1	1	1	1	1	1	1	1	1	1	1	1	0	1	1	1	0	0	1	0	1	0	1	0
d	1	0	1	1	0	1	1	0	1	1	0	1	0	0	0	1	0	0	0	1	1	1	1	0
e	0	0	0	0	1	0	0	0	0	0	1	0	0	0	0	0	1	0	0	1	1	0	1	0
F	1	1	1	1	1	1	1	1	1	1	1	1	1	1	1	1	1	1	1	1	1	1	1	1

Note: (0 = non-convertible; 1 = convertible. a–f represent cropland, forestland, grassland, water bodies, construction land, and unused land, respectively).

Field weight represents the expansion intensity of different land use types, with a value range of 0 to 1 (Table 3). The closer the value is to 1, the stronger the expansion capability; conversely, the closer it is to 0, the weaker the expansion ability [57]. The specific formula is as follows:

$$X_i = (\Delta TA_i - \Delta TA_{min}) / (\Delta TA_{max} - \Delta TA_{min}) \quad (12)$$

Table 3. The domain weights in the Yarlung Zangbo River Basin under four scenarios.

Type	Cropland	Forest Land	Grassland	Water Body	Construction Land	Unused Land
NDS	0.551	0.220	0.221	0.100	1.000	0.243
CPS	0.370	0.328	0.315	0.100	1.000	0.458
EPS	0.722	0.327	1.000	0.100	0.983	0.412
UDS	0.535	0.212	0.221	0.100	1.000	0.180

In the equation, X_i represents the field weight parameter for the i-th land use type; ΔTA_i denotes the change in the *i-th* land use type; and ΔTA_{max} and ΔTA_{min} represent the maximum and minimum changes, respectively.

3. Results

3.1. Characteristics of Land Use Type Changes

As shown in Table 4 and Figure 4, the land use composition of the YZRB during 2000–2020 was dominated by grassland, forest land, and unused land, collectively occupying more than 94.0% of the total area. The area of construction land constituted the smallest proportion (<1%). Except for forest land, whose area showed a decreasing trend, the area proportion of all other land types increased. Cropland in the YZRB remained spatially constrained (mean area = 3900.44 km^2), peaking at 4121.81 km^2 (2020) with a cumulative gain of 672.3 km^2. The most significant expansion occurred during 2005–2010 (Δ+813.44 km^2, +23.67%), followed by a marked contraction (Δ−121.07 km^2) in 2015–2020, reflecting intensified reclamation pressures. Its proportional coverage increased from 1.28% (2000) to 1.52% (2020). Concurrent land transitions revealed divergent trajectories: Forest land expanded from 45,684.47 km^2 (16.92%) to 62,621.18 km^2 (23.16%), indicating afforestation initiatives (Δ+16,936.71 km^2). Grassland (basin-dominant at >46%) declined persistently (Δ−35,607.6 km^2), from 160,398.80 km^2 to 124,791.20 km^2.Water body maintained equilibrium states (fluctuating around 11,587.51 km^2). Construction land exhibited accelerated urbanization (Δ+261.31 km^2), proportionally increasing from 0.04% to 0.10%. Unused land increased by 19,250.04 km^2, signaling land degradation pressures.

Table 4. Land use patterns in the Yarlung Zangbo River Basin from 2000 to 2020(km^2).

Land Use Type	Year					Single Dynamic Degree/%
	2000	2005	2010	2015	2020	2000–2020
Cropland	3449.51	3437.27	4250.71	4242.88	4121.81	0.97
Forest land	45,684.47	45,691.02	62,680.46	62,665.45	62,621.18	–3.05
Grassland	160,398.80	160,374.80	124,851.60	125,230.90	124,791.20	–1.11
Water body	12,268.27	12,277.18	11,117.16	11,178.81	11,096.12	–0.48
Construction land	118.17	144.38	172.31	179.63	379.47	11.06
Unused land	48,136.84	48,133.11	67,321.30	66,869.17	67,386.88	2.00

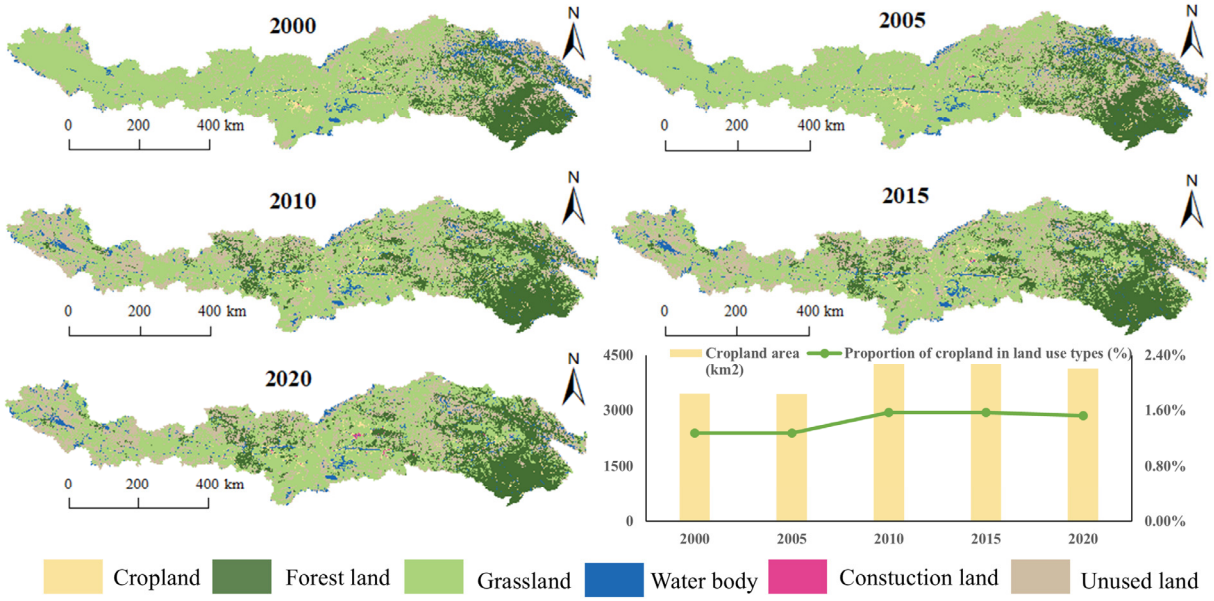


Figure 4. The land use types in the Yarlung Zangbo River Basin from 2000 to 2020.

The annual change intensity index (Table 4) quantified these dynamics: Cropland showed biphasic trends (peak Δ = +4.73% during 2000–2020; nadir Δ= −0.57%

in 2015–2020), with an aggregate increase (0.97%/yr). Construction land maintained positive growth ($\Delta > 0$ throughout). Grassland and water body displayed negative indices ($\Delta < 0$). Forest land transitioned from positive gains (2000–2010) to loss phases (2010–2020). Unused land demonstrated sustained expansion ($\Delta > 0$), indicative of underutilized land accumulation.

3.2. Land Use Transition Matrix Analysis

Land use transition matrix analysis was applied to quantify cropland dynamics in the YZRB during 2000–2020. As shown in Figure 5, the area of cropland decreased between 2000 and 2005, mainly due to its conversion to grassland (47.14 km^2) and forest land (17.77 km^2). From 2005 to 2010, the cropland area increased, primarily through conversions from grassland (957.32 km^2) and forest land (561.32 km^2). During 2010–2020, the area exhibited a decreasing trend again, with cropland mainly converted to forest land, grassland, and water bodies. Overall, the changes in cropland area during each period were largely driven by mutual conversions with grassland and forest. Between 2000 and 2020, results (Figure 5) reveal bidirectional transitions among all land categories, with net areal expansion in cropland (+670.16 km^2), forest land (+16,898.52 km^2), construction land (+261.30 km^2), and unused land (+19,120.08 km^2), alongside contraction of grassland (−35,659.63 km^2) and water body (−1290.44 km^2). The cropland gain (2661.99 km^2) primarily originated from grassland conversions (1907.32 km^2, 71.7%) and forest land transitions (489.19 km^2, 18.4%). Conversely, cropland loss (1991.83 km^2) was dominated by natural revegetation (grassland: 979.96 km^2, 49.2%; forest: 552.36 km^2, 27.7%) and hydrological encroachment (water body: 214.85 km^2, 10.8%).

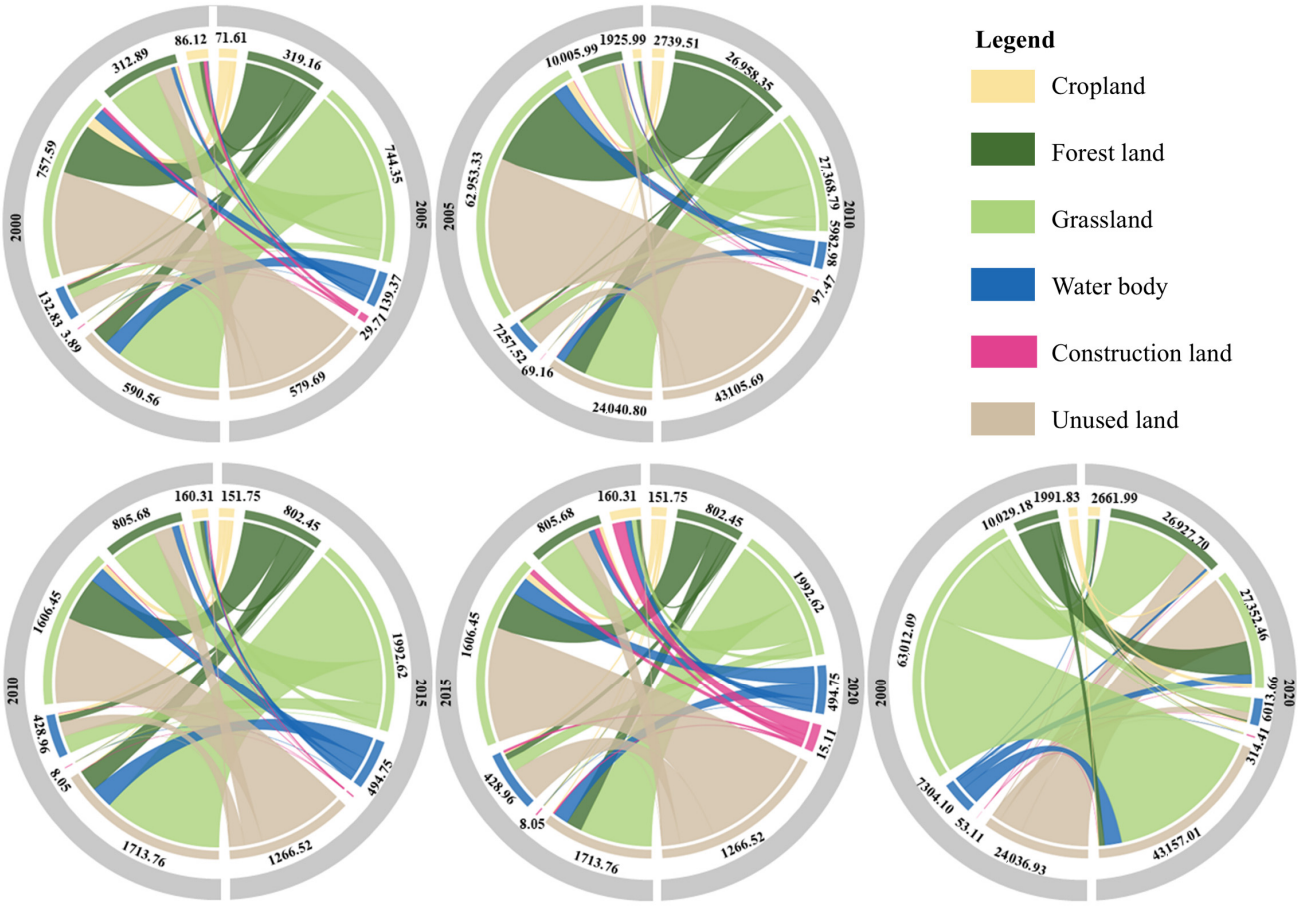


Figure 5. Land use change in the Yarlung Zangbo River Basin from 2000 to 2020.

3.3. Center of Gravity Shift and Standard Deviation Ellipse

The centroid displacement model was applied to quantify spatiotemporal shifts in cropland gravity centers across temporal intervals (2000–2020), with trajectory mapping (Figure 6) revealing consistent northwest–southeast orientation, indicating high spatial clustering within the YZRB. Topographic gradients establish a bioclimatic transition from humid subtropical to semi-arid continental regimes. The northwestern core encompasses the Rikaze alluvial plains (mid-upper YZRB), including the Year Chu River and Lhasa River basins and broad valleys supporting Tibet's primary agricultural belt (>70% basin-scale cropland in contiguous parcels). In contrast, the southeastern Linzhi gorge systems (Dri Chu-Nyang River Basin) exhibit humid subtropical climates with fragmented cultivation on steep fluvial terraces due to gorge-confined topography. Cropland centroids clustered within the Zhanang County-Naidong District-Qiongjie County nexus demonstrated phased displacement: northwestward shift and northwestward reversion.

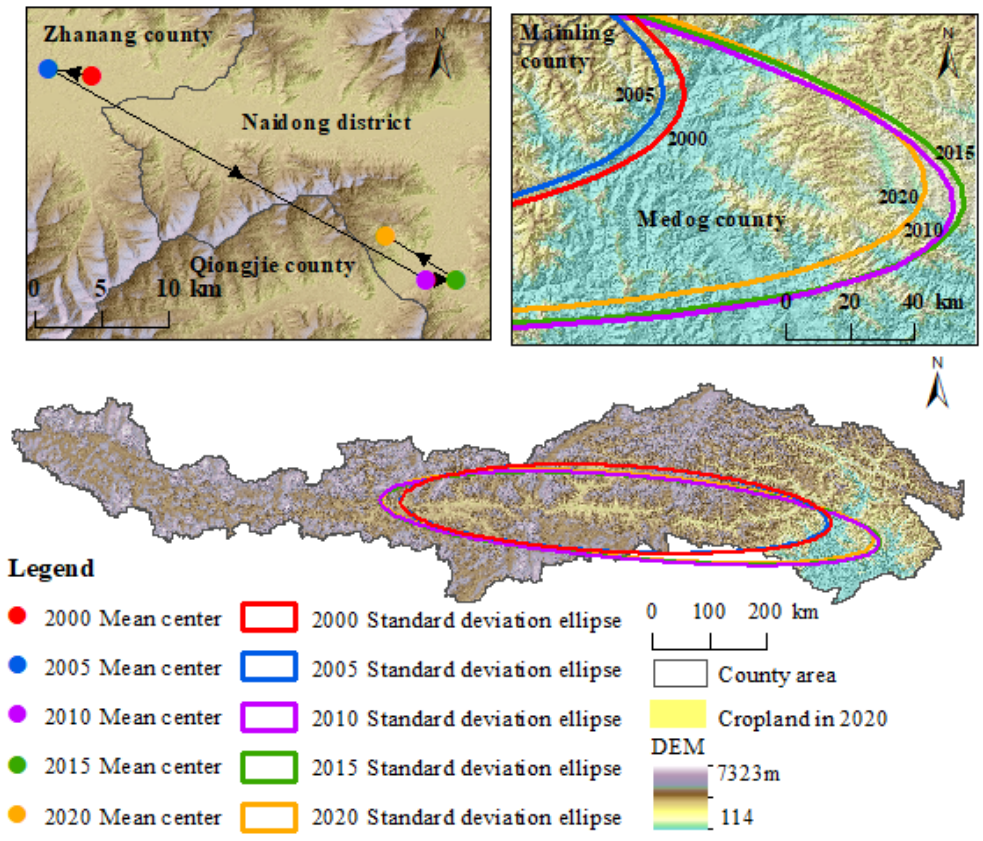


Figure 6. Elliptical shift and centroid shift.

The standard deviational ellipse (SDE) analysis (Figure 6 and Table 5) reveals biphasic spatial dynamics in cropland distribution: initial dispersion (2000–2020) marked by increasing major axis length (326.67 km→375.46 km) and subsequent clustering (2000–2020) with reduced dispersion (−2.56 km minor axis contraction). Ellipse orientation remained persistently northwest–southeast (ellipticity $\geq$ 0.77), aligning with centroid migration trajectories. The mean ellipse area (83,320.05 km^2) and perimeter (1507.38 km) exhibited an overall increase, reflecting scale–dependent expansion patterns linked to topographically constrained cultivation intensification.

Table 5. The changes in standard deviation ellipse parameters of cropland in the Yarlung Zangbo River Basin from 2000 to 2020.

Year	2000	2005	2010	2015	2020
Major Axis Standard Deviation (km)	326.67	323.77	380.83	381.59	375.46
Minor Axis Standard Deviation (km)	76.22	75.86	73.28	72.43	73.66
Rotation Angle (°)	101.38	101.41	103.59	103.35	103.24
Area (km^2)	78,194.28	77,133.50	87,631.46	86,797.27	86,843.72
Perimeter (km)	1390.99	1379.24	1595.08	1596.68	1574.91
Flattening	0.77	0.77	0.81	0.81	0.80

3.4. Cropland Change Driving Force Analysis

3.4.1. Correlation Analysis Between Driving Factors and Cropland Area

Prior to Partial Least Squares Structural Equation Modeling (PLS-SEM) implementation, a correlation analysis was first performed between the 10 driving factors and the areas of cropland increase and decrease. A normality test was carried out on the data, which revealed that the data did not meet the normal distribution assumption. Therefore, Spearman's correlation analysis was employed. Figure 7 displays the variability in the correlation between the areas of cropland increase and decrease and the driving factors from 2000 to 2020.

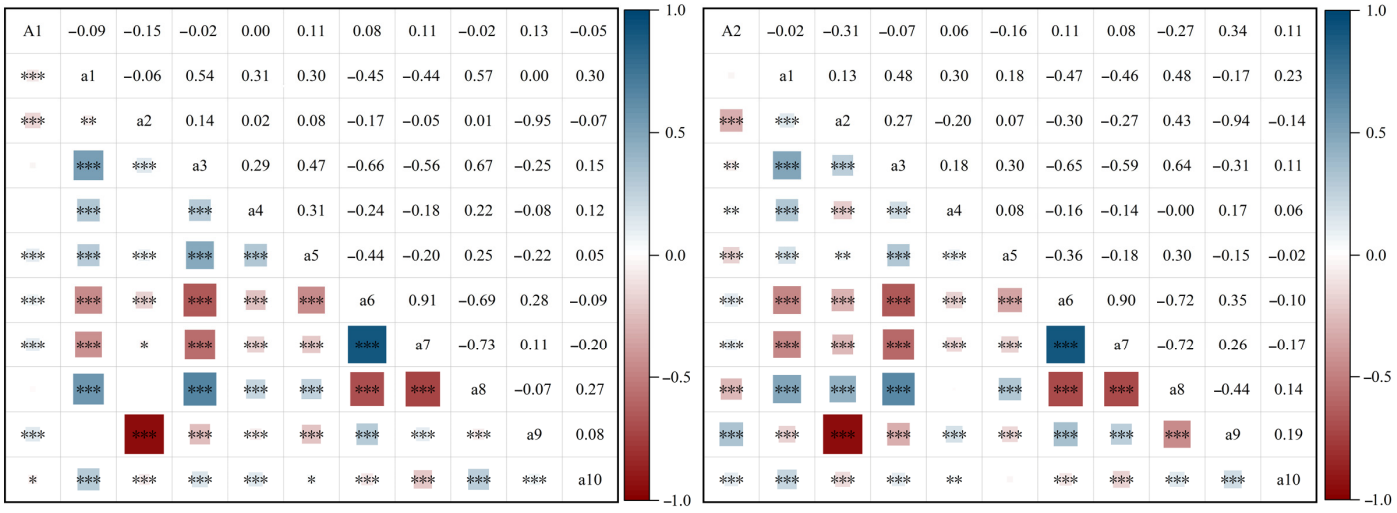


Figure 7. Interaction and correlation between the increased and decreased areas of cropland and different driving factors. ($p < 0.05$ (*), $p < 0.01$ (**), $p < 0.001$ (***). A1: cropland gain area; A2: cropland loss area; a1: distance to secondary road; a2: temperature; a3: distance to tertiary road; a4: Slope; a5: precipitation; a6: population; a7: GDP; a8: distance to primary road; a9: DEM; a10: distance to water body).

The results show that, at a confidence level of $p = 0.001$, annual precipitation, population density, GDP, and elevation are positively correlated with the area of cropland increase (ρ = +0.111, +0.08, +0.11, +0.13). Conversely, the distance to secondary roads, average annual temperature, distance to tertiary roads, distance to primary roads, and distance to water bodies are negatively correlated with the area of cropland increase (ρ = −0.09, ρ = −0.15, −0.02, −0.02, −0.05). Additionally, the distance to tertiary roads, slope, and distance to primary roads showed no or weak correlations with the area of cropland increase.

Slope, population density, GDP, elevation, and distance to water body show a significant positive correlation with the area of cropland decrease(ρ = +0.11, +0.08, +0.34, +0.11), while distance to secondary roads, average annual temperature, distance to tertiary

roads, annual precipitation, and distance to primary roads exhibit a significant negative correlation with the area of cropland decrease(ρ = −0.02, −0.31, −0.07, −0.16, −0.27). Among these, elevation has the strongest correlation with the area of cropland decrease (ρ = +0.34), at a confidence level of p = 0.001, indicating a significant positive correlation. The correlation coefficient for average annual temperature and cropland decrease is −0.31, indicating a significant negative correlation.

Multivariate analysis highlights elevational gradients, thermal regimes, and socioeconomic drivers (population/GDP) as dominant controls over cropland transitions. Spatial planning strategies should prioritize road network optimization, microclimate adaptation, and demographic–economic coordination to balance agricultural intensification with ecological sustainability.

3.4.2. Analysis of Driving Factors Based on PLS-SEM

To disentangle the complex interdependencies between cropland dynamics and multidimensional drivers, we employed PLS-SEM to quantify the direct and mediated effects of natural factors (annual precipitation, average annual temperature, elevation, slope), socioeconomic factors (population density, GDP), and proximity factors (distance to primary/secondary/tertiary roads, water body). The PLS-SEM framework was constructed under three hypothesized causal pathways:

(1) Natural factors, socioeconomic factors, and proximity factors directly influence changes in cropland area;
(2) Natural factors indirectly influence cropland area changes through their impact on proximity and socioeconomic factors;
(3) Socioeconomic factors indirectly influence cropland area changes through their effect on proximity factors.

The R^2 value indicates that the model's fit is within an acceptable range, and the positive Q^2 value demonstrates that the model performs well in predicting endogenous latent variables [58]. The AVE values are all greater than 0.5, suggesting that the variance explained by the latent variables exceeds the error, indicating good convergent validity of the measurement model. The GOF value indicates that the model provides a good overall fit to the data, effectively revealing the relationships between the variables [59]. All path coefficients exhibited high statistical significance ($p \leq 0.001$), validating the hypothesized causal architecture (Table 6).

Table 6. Model performance of PLS-SEM. ($p < 0.01$ (**), $p < 0.001$ (***).).

Model Performance Indicators	Type	Value (Cropland Increase)	Value (Cropland Decrease)	Standard	Description
R^2	Socioeconomic factors	0.001	0.000	>0.67	Substantial explanatory power
	Proximity factors	0.546	0.811	>0.33	Moderate explanatory power
	/	/	/	>0.19	Weak explanatory power
Q^2	Socioeconomic factors	0.002	0.001	>0	A larger value denoting higher prediction accuracy of the model
	Natural factors	0.000	0.000		
	Proximity factors	0.373	0.554		
AVE	Socioeconomic factors	0.995	0.999	>0.5	A higher value indicates better convergent validity of the model
	Natural factors	0.513	0.503		
	Proximity factors	0.717	0.701		

Table 6. *Cont.*

Model Performance Indicators	Type	Value (Cropland Increase)	Value (Cropland Decrease)	Standard	Description
p–value	Socioeconomic factors-Cropland	0.000 ***	0.000 ***	≤0.001	Statistically significant
	Natural factors-Cropland	0.001 **	0.000 ***		
	Proximity factors-Cropland	0.000 ***	0.000 ***		
GOF	/	0.385	0.486	0.1	Weak model fitting
	/			0.25	Medium model fitting
	/			0.36	Strong model fitting

3.4.3. Impact of Latent and Manifest Variables on Cropland Area Change

PLS-SEM path coefficients elucidate the direct and mediated effects of latent variables on cropland dynamics (2000–2020) (Figure 8)

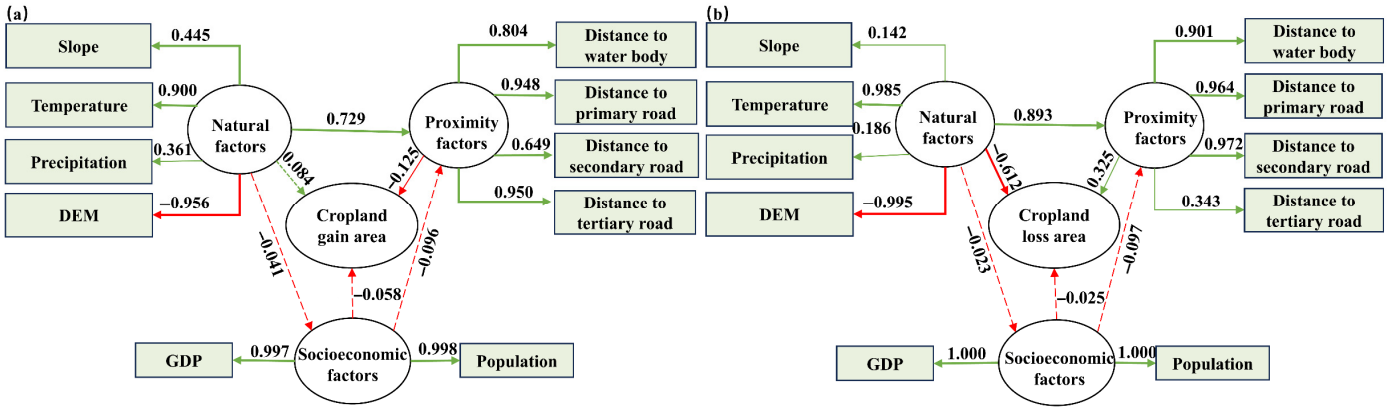


Figure 8. Relationship between each driving factor and the increased and decreased areas of cropland from 2000 to 2020 based on the PLS-SEM model. (Green and red lines indicate positive and negative path coefficients, respectively. The strength of the coefficients is visualized by line styles: bold lines for absolute values greater than 0.4, thin lines for values between 0.1 and 0.4, and dashed lines for values less than 0.1. (**a**) depicts the relationship between driving factors and the increased area of cropland from 2000 to 2020, while (**b**) shows the relationship between driving factors and the decreased area of cropland during the same period (2000–2020)).

Natural drivers (natural factors): weak direct positive effect on land gain (β= +0.084), predominantly mediate through accessibility metrics (βindirect = +0.729), reflecting topography-filtered cultivation expansion. Accessibility constraints (proximity factors): direct negative impact on land gain (β = −0.125); amplify socioeconomic pressures (β = −0.096), exacerbating human–induced fragmentation. Socioeconomic pressures (population/GDP): direct suppression of land gain (β = −0.058), indirectly constraining agricultural intensification via accessibility (βindirect = −0.21).

For cropland loss: natural drivers strongly inhibit reduction (β = −0.612), mediated by accessibility (βindirect = +0.34); accessibility metrics promote abandonment (β = +0.28), while socioeconomic factors mitigate loss (β = −0.17).

In summary, proximity factors have the greatest impact on cropland area change, followed by natural factors. Proximity factors exert a negative impact on the increase in cropland area, while natural factors have a positive effect on the increase in cropland area.

3.5. Cropland Landscape Distribution in 2030 Under Different Scenarios

Based on land use data from 2000 and 2010 in the Yarlung Zangbo River Basin, the 2020 land use classification distribution of the study area was simulated using the LEAS

and CARS modules of the PLUS model, combined with consistent landscape development probability parameters at 10-year intervals. Validation was carried out by comparing the actual 2020 land use type data with the simulated data. The results showed that the Kappa coefficients for the simulation in the NDS, CPS, EPS, and UDS were 0.969, 0.930, 0.977, and 0.976, respectively. The Kappa coefficients are greater than 0.75, making it suitable for simulating land use patterns in the Yarlung Zangbo River Basin [60–62]. The OA values were 0.979, 0.954, 0.984, and 0.984, and the FoM values were 0.126, 0.078, 0.072, and 0.081, indicating that the simulation accuracy reached an ideal state and the simulation reliability was high [63]. The 2030 land use distribution in the Yarlung Zangbo River Basin was simulated using landscape development probability parameters derived from 10-year intervals, providing a foundational basis for establishing the spatial land use pattern of the basin in 2030. The precision, recall, and F1-scores of cropland under each simulated scenario are presented (Figure 9). The PLUS model achieved an F1-score greater than 0.90 for cropland, with both precision and recall exceeding 0.90, indicating a relatively balanced performance. The F1-scores of different land use types varied significantly across the NDS, CPS, EPS, and UDS methods. Built-up land showed the lowest F1-scores (all <0.6), much lower than other types (mostly > 0.9), reflecting an imbalance with high precision and low recall. Forest and grassland performed well, with both precision and recall above 0.95. The UDS method achieved the best overall performance, with F1-scores near 0.99 for most natural land types. However, it showed low precision and high recall for built-up land. Further improvements can be made by enhancing data, adding features, or adjusting model thresholds. These results suggest that the model demonstrates a certain level of reliability in identifying cropland in the Yarlung Zangbo River Basin under the 2030 land use simulation. Figure 10 shows the simulated spatial distribution of land use in the Yarlung Zangbo River Basin under four different scenarios for the year 2030. Table 7 shows the changes in cropland area under the four projected scenarios for 2030, compared with the actual cropland area in 2020.

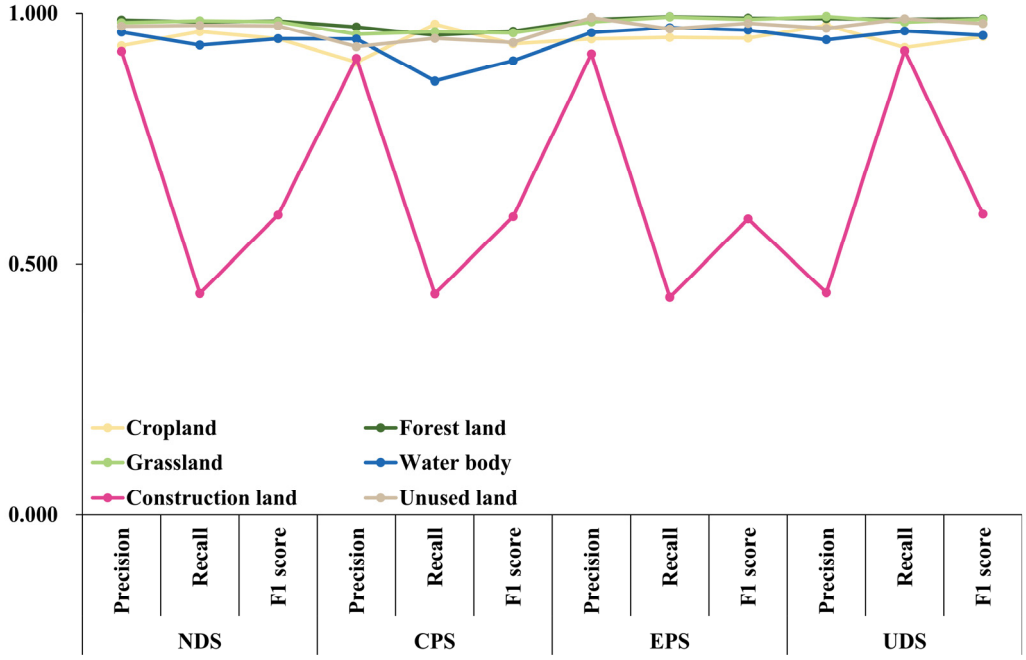


Figure 9. Precision, recall, and F1-scores under four scenarios. (NDS: natural development scenario; CPS: cropland protection scenario; EPS: ecological protection scenario; UDS: urban development scenario).

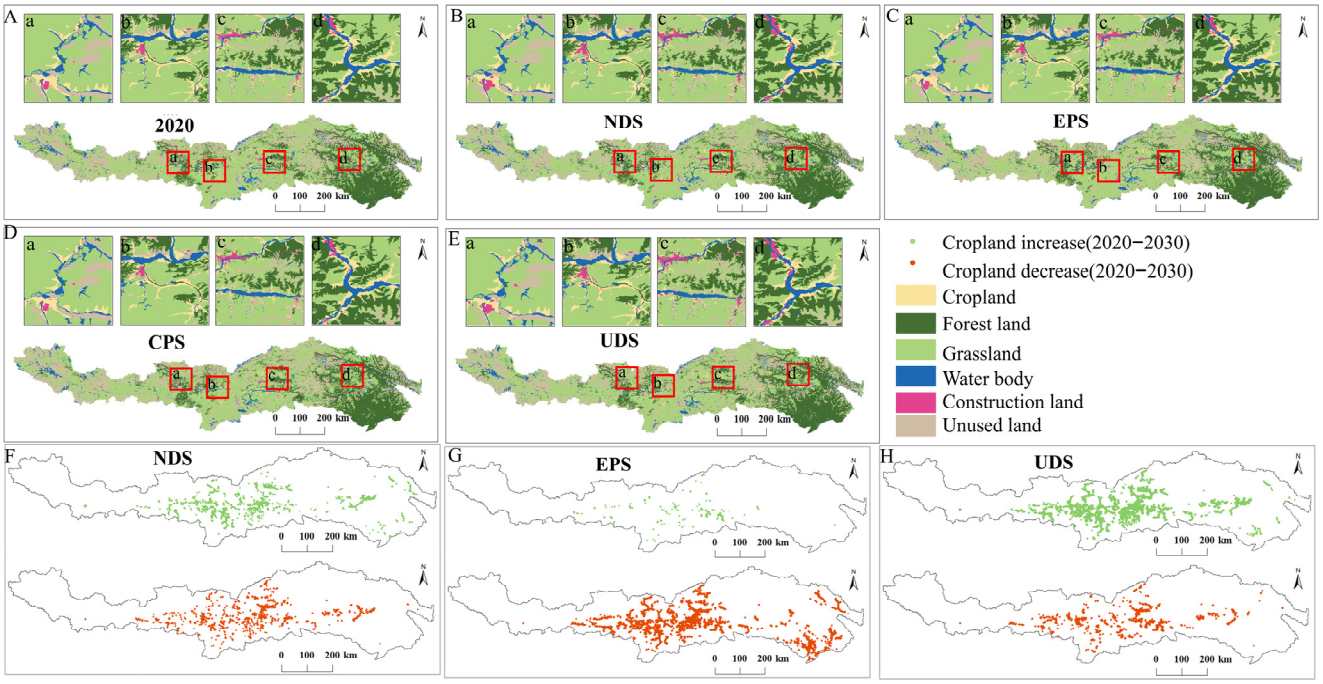


Figure 10. Simulated Spatial Distribution of Land Use under Four Scenarios in the Yarlung Zangbo River Basin in 2030 and the Cropland Gain–Loss Distribution from 2020 to 2030 (NDS: natural development scenario; CPS: cropland protection scenario; EPS: ecological protection scenario; UDS: urban development scenario; (**A**) shows the actual land use distribution in 2020. (**B**–**E**) present the predicted land use distributions under four scenarios(NDS, EPS, CPS, UDS) in 2030. (**F**–**H**) respectively illustrate the distribution of cultivated land increase/decrease under each scenario (NDS, EPS, UDS) compared with 2020. a–d indicate areas with significant changes; no cropland change map is shown for the 2030 cropland protection scenario as it is identical to the 2020 situation. In panel (**H**), the increase in cropland is not visually prominent due to pixel overlap (with 452,638 pixels gained and 327,486 pixels lost).

Table 7. Changes in the area of cropland under the four predicted scenarios for 2030 compared to the actual cropland area in 2020. (km^2, NDS: natural development scenario; CPS: cropland protection scenario; EPS: ecological protection scenario; UDS: urban development scenario; CR: Change rate).

Type	2020	NDS		CPS		EPS		UDS	
	Area	Area	CR (%)	Area	CR (%)	Area	CR (%)	Area	CR (%)
Cropland	4121.81	4002.92	−2.88	4121.42	−0.01	4002.92	−2.88	4006.15	−2.81
Forest land	62621.18	62567.50	−0.09	62620.75	0.00	63315.21	1.11	62508.13	−0.18
Grassland	124791.20	124663.97	−0.10	124787.11	0.00	124746.83	−0.04	124663.97	−0.10
Water body	11096.12	10933.97	−1.46	11095.66	0.00	11135.93	0.36	10933.97	−1.46
Construction land	379.47	515.66	35.89	379.36	−0.03	414.40	9.21	571.79	50.68
Unused land	67386.88	67280.78	−0.16	67385.62	0.00	66349.52	−1.54	67280.78	−0.16

3.5.1. Natural Development Scenario (NDS)

Projected cropland area decreases by 118.89 km^2 (−2.88%), with concurrent declines in all land categories except construction land. Urban expansion concentrates in Sangzhuzi, Duolongdeqing, Chengguan, and Naidong districts, reflecting unrestricted land conversion under baseline trajectories. This unregulated pathway threatens both agroecological systems and ecosystem services, necessitating urgent policy interventions.

3.5.2. Cropland Protection Scenario (CPS)

Under the cropland protection scenario, compared to the natural development, ecological protection, and urban development scenarios, the cropland area increases by 118.51 km^2,

118.51 km^2, and 115.27 km^2, respectively. Spatial clusters emerge in southern Lhasa and the core agricultural zones of Rikaza, Shannan, and Linzhi (Sangzhuzi, Duolongdeqing, etc.). While artificial surface expansion persists, CPS effectively curtails cropland loss without compromising forest/grassland integrity, balancing food security and ecological resilience.

3.5.3. Ecological Protection Scenario (EPS)

Cropland reduction mirrors NDS (−2.88%), but diverges through forest land (+1.11%) and water body (+0.36%) gains. Construction land growth decelerates sharply (35.89% → 9.21%), though insufficient cropland safeguards persist. Grassland (−0.04%) and unused land losses highlight trade-offs between conservation priorities and agricultural sustainability.

3.5.4. Urban Development Scenario (UDS)

Accelerated urbanization drives a construction land surge (+192 km^2, +50.68%), concentrated in Lhasa's southern periphery and Rikaze-Shannan-Linzhi corridors. Cropland plummets to 4006.15 km^2 (−115.66 km^2 vs. 2020), with parallel declines in other land categories. This pathway exacerbates agroecological fragmentation, underscoring the incompatibility between unchecked urban growth and regional sustainability goals.

4. Discussion and Conclusions

4.1. Discussion

4.1.1. Spatiotemporal Dynamics of Cropland

The YZRB exhibits a land cover composition dominated by grasslands (51.48%), unused land (22.04%), and forest land (20.67%), with cropland occupying merely 1–2% of the basin yet sustaining > 70% of Tibet's agricultural output. From 2000–2020, cropland exhibited net expansion (0.97%/yr), primarily through conversions from grassland (1907.32 km^2) and forest (489.19 km^2), while losses stemmed from natural revegetation (grassland: 979.96 km^2; forest: 552.36 km^2) and hydrological encroachment (water body: 214.85 km^2). Spatial clustering intensified, as evidenced by centroid convergence (SDE ellipticity $\geq$ 0.77) toward the Zhanang-Qiongjie-Naidong nexus (NW–SE orientation), reflecting topographic constraints and valley-dependent cultivation patterns. Compared to other basins [64–66], the YZRB shows significant dependence on river valley croplands, which are mainly located in relatively low–altitude areas. Due to the limitations of the plateau terrain, the croplands are often scattered in small, patchy distributions on both sides of the river valley, with small and discontinuous scales.

In the context of increasingly frequent extreme weather events and a significant rise in global temperatures, high-altitude regions such as the Yarlung Zangbo River Basin have experienced notable environmental shifts. The basin's valley areas, situated at elevations ranging from 3000 to 4000 m, were historically constrained by low temperatures, which limited the expansion of cropland. However, climate warming has led to increases in accumulated temperature, effectively extending the growing season. This has created favorable conditions for cultivation in previously unsuitable high-altitude grasslands and forested areas. Our results indicate that cropland expansion has predominantly resulted from the conversion of grassland (1907.32 km^2) and forest (489.19 km^2), both of which are mainly distributed in higher elevation zones. This spatial pattern suggests that climate warming may be a key driver facilitating the transition of these ecosystems into arable land. The transformation aligns with broader regional land use dynamics shaped by climate–induced agricultural potential. Moreover, the increasing emphasis on food security and the implementation of land protection policies have jointly contributed to the stabilization and growth of cropland area. These factors may have acted synergistically with climatic changes, reinforcing the expansion trend in high-altitude agricultural landscapes.

"Cropland is the carrier of permanent basic cropland, and permanent basic cropland is the core object of cropland protection." YZRB's cropland dynamics directly impact regional food security under China's "triple objectives" (no area reduction, no use change, quality improvement). Strategic interventions like the High-Standard Cropland Construction Initiative aim to mitigate non-agriculturalization risks through land–use zoning and ecological compensation mechanisms.

4.1.2. Factors Driving Cropland Area Changes

The study employs a multidimensional analytical approach by constructing a comprehensive research framework that integrates bivariate correlation analysis and partial least squares structural equation modeling (PLS-SEM). This framework aims to reveal the complex interaction mechanisms of natural factors, proximity factors, and social–economic factors on cropland change.

The increase in cropland area shows a significant positive correlation with annual precipitation ($\beta = 0.11$), population ($\beta = 0.08$), and GDP ($\beta = 0.11$), indicating that abundant rainfall, high population density, and advanced economic development are more conducive to the protection of cropland. The results of cropland expansion in the basin are consistent with the findings of [67–69]. Among the topographic factors, the positive correlation with elevation($\beta = 0.13$) reflects that mid- to low–elevation areas are more suitable for the expansion of farming systems [10]. In contrast, accessibility and thermal conditions exhibit a significant negative correlation, suggesting that infrastructure expansion and thermal stress have a suppressive effect on the persistence of cropland [70]. The process of cropland loss shows a differentiated response mechanism, where slope, distance to water body, and economic development intensity form a significant positive driving force($\beta = 0.06$, $\beta = 0.11$, $\beta = 0.18$), validating the extrusion effect of urban land expansion on cropland [71]. Notably, the elevation factor demonstrates the strongest explanatory power in cropland loss ($\beta = 0.34$), revealing the critical role of topographic constraints in the sustainable use of cropland [72,73].

The PLS-SEM model analysis reveals that natural factors have a weak direct impact on cropland expansion, but they exert a significant indirect effect through proximity factors, indicating that natural conditions indirectly regulate the cropland expansion process through locational factors [74]. Socioeconomic factors exhibit a bidirectional modulation characteristic: although the system path coefficient is negative ($\beta = -0.058$), the local positive effects of population density and GDP are significant($\beta = 0.997$, $\beta = 0.998$), reflecting the structural contradiction between cropland protection and demand growth during economic development [75]. Proximity factors have a significant global impact on cropland loss ($\beta = 0.325$), with the distance to secondary roads being particularly influential in driving land loss ($\beta = 0.972$). This confirms the applicability of the "transport–oriented development" theory in land conversion, where the radiation effect of road infrastructure accelerates land use transformation in surrounding areas [76,77].

Based on a comparative analysis of standardized path coefficients, natural and proximity factors constitute the dominant driving forces, while socioeconomic factors are secondary. Future efforts should focus on land use planning along transportation corridors and near water bodies, improving the cropland protection system within transportation corridor buffer zones, and establishing a linkage mechanism between road construction and cropland occupation compensation. Additionally, a cropland expansion priority area identification system based on heat–precipitation coupling suitability evaluation should be developed. This will help balance natural conditions with socioeconomic development, ensuring the sustainable protection of cropland resources while meeting the demands of economic development.

Significant factors influencing cropland change identified by the PLS-SEM model—such as elevation and precipitation among natural factors, population and GDP among socioeconomic factors, and distances to roads and water bodies among proximity factors—were incorporated as key driving variables in the PLUS model simulation. These factors are closely associated with cropland dynamics and align well with the PLUS model's requirements for driving factor selection.

4.1.3. Multi-Scenario Simulation of Cropland in 2030

The PLUS model was used to simulate the spatial distribution of cropland in the YZRB under four scenarios for 2030: natural development, cropland protection, ecological protection, and urban development. This model reveals the trends of land use changes in the YZRB under these four scenarios. All four scenarios show a reduction in cropland and grassland areas, with construction land decreasing in the cropland protection scenario (whereas it sharply increases in the other scenarios). In comparison to the other three scenarios, the cropland protection scenario ensures the total amount of cropland is maintained, while ecological land is protected, and the expansion of construction land is somewhat restricted. This simulation result is more consistent with the sustainable development of the study area and aligns with the trends observed in [78]. As a key grain production area on the Qinghai-Tibet Plateau, the YZRB has been facing dual pressures of decreasing cropland and "non-agriculturalization" in recent years. Urban expansion, tourism development, and the cultivation of traditional Tibetan medicinal herbs have contributed to the continued loss of cropland, threatening the inheritance of the Tibetan farming culture and food security. The main crop in the basin is *barley* (*Qingke*), which is not only a traditional staple food and beverage (such as *Zanba* and *barley wine*, irreplaceable in religious festivals and daily diets) but also a core component of the farming culture. The area and yield of *barley* are directly related to cultural heritage and food security. Although the *barley* production in Tibet increased from 637,100 tons in 2012 to 888,000 tons in 2024 (an average annual growth rate of 3.0%), the non-agriculturalization of cropland will be a significant limiting factor for future overall growth. As cropland becomes "non-agriculturalized," the space for *barley* cultivation is compressed, which could lead to the potential loss of related artisanal skills (such as *Zanba* production) due to unstable raw material supplies. This, in turn, may reduce the younger generation's identification with traditional diets, threatening cultural heritage. Meanwhile, shifting to non-food crops (such as Tibetan medicinal herbs) may yield high short–term profits, but it could degrade soil structure and threaten the long-term sustainability of regional agriculture, thereby endangering regional food security.

According to the Ecological Protection Law of the Qinghai-Tibet Plateau, both the ecological protection red line and permanent basic farmland (In China, "farmland" specifically refers to cropland (Class 01) as defined in the Current Land Use Classification standard. It corresponds exactly to "cropland" and excludes other agricultural land types such as pastures and orchards, as well as recreational plots. Reasonable seasonal use is permitted within this classification.) are part of the country's "three control lines" (ecological red line, permanent basic farmland, and urban development boundaries). High-quality cropland in valley areas (such as the Linzhi section) constitutes the main body of permanent basic farmland. In 2020, an area of up to 2024.83 km^2 of cropland was designated as permanent basic farmland, forming a "misaligned (crossed) protection" pattern with the ecological protection red line, ensuring both food production and reduced ecological pressure. The overlapping area between the ecological protection red line and cropland in the YZRB in 2020 was 344.77 km^2. The area of cropland within a 500-m buffer zone was 775.52 km^2, and within a 100-m buffer zone, it was 415.30 km^2. In the Yarlung Zangbo River Black-necked Crane Nature Reserve, the black-necked cranes frequently forage in cropland, and the

post-harvest dryland fields provide abundant food sources for them, with the foraging time accounting for about four-fifths of their total foraging time. At the same time, there is partial overlap between the ecological protection red line and permanent basic farmland in the study area, with an overlapping area of 491.99 km^2. Local conflicts may be addressed through ecological compensation mechanisms (such as economic compensation for farmers who retire from farming) or through the improvement of cropland quality (such as constructing high-standard cropland), achieving a win–win situation. The core objective of nature reserves is to protect typical ecosystems and endangered species, which aligns well with the ecological function of the ecological protection red line. Nature reserves within the Yarlung Zangbo River Basin (such as the Yarlung Zangbo Grand Canyon National Nature Reserve) are often directly included within the ecological protection red line, with some permanent basic farmland integrated into the reserves, promoting a harmonious coexistence between humans and nature. Figure 11 illustrates the spatial distribution of cropland (2020), permanent basic farmland, nature reserves, and ecological conservation redlines in the Yarlung Zangbo River Basin.

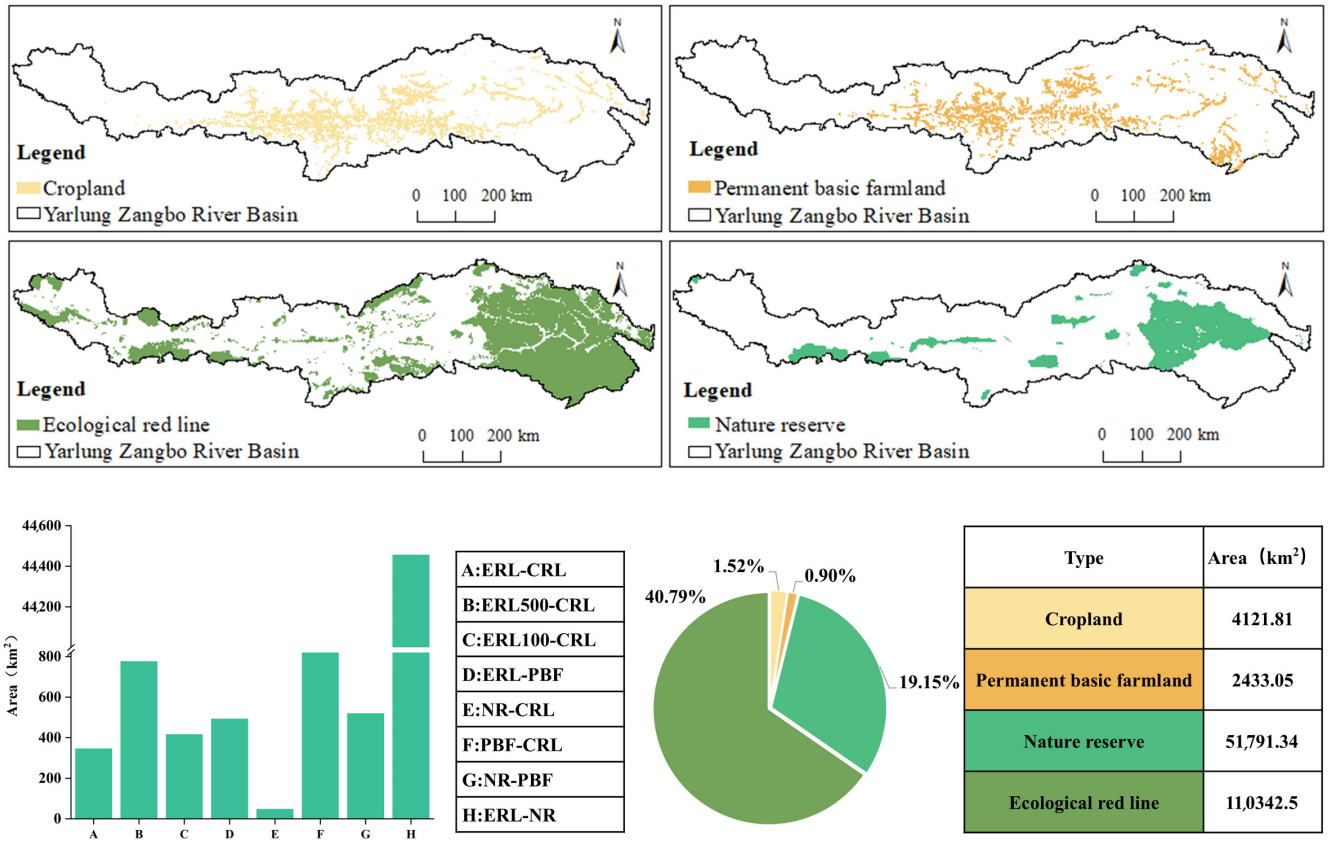


Figure 11. Distribution of cropland (2020), permanent basic farmland, nature reserves, and ecological red line in the Yarlung Zangbo River Basin. The bar chart represents the overlapping area of each land type. Cropland is represented as CRL, permanent basic farmland as PBF, nature reserves as NR, ecological red line as ERL, ERL500 as the 500-m buffer zone of the ecological red line, ERL100 as the 100-m buffer zone of the ecological red line, and ERL-CRL as the overlapping area between ERL and CRL. Similar abbreviations are used for subsequent areas. The pie chart shows the proportion of each land type in relation to the total area of the Yarlung Zangbo River Basin.

4.1.4. Limitations of the Study

The chain effects of climate change and human activities on the spatiotemporal variation in impacts will become increasingly stronger in the future [79]. Climate-induced risks—such as warming, extreme weather, and water resource fluctuations—may reduce

agricultural suitability and accelerate the abandonment of marginal croplands. Additionally, glacier melt-induced runoff changes threaten the sustainability of irrigation systems. Indirect impacts also arise from human adaptation strategies, including labor migration driven by declining agricultural productivity, which leads to extensive land management or cropland abandonment. Future research should investigate the micro-level mechanisms of cropland abandonment and develop differentiated strategies, such as promoting smart agriculture in core areas, encouraging cropland tourism development in suburban zones, and establishing fallow warning systems in ecologically fragile regions. Moreover, urban expansion and ecological land retirement policies further compress cropland availability, while tourism–driven land conversion (e.g., homestays, scenic spot development) increases the risk of encroachment. Understanding the trajectory of cropland change under different policy interventions, while integrating cultural perspectives, could improve the precision and adaptability of land management strategies.

In terms of modeling limitations, the PLUS model yielded poor F1-scores for built-up land (generally < 0.6), indicating a precision–recall imbalance. Although the UDS performed well for natural land categories (F1 ≈ 0.99), it exhibited the opposite issue for built-up areas—high recall but low precision. Future work should address this imbalance through data augmentation, feature enhancement, or threshold tuning. In the PLS-SEM model, some variables exhibited severe multicollinearity, indicating a need for further refinement and validation of the structural paths. Lastly, this study did not assess prediction uncertainty—such as error bounds, sensitivity analysis, or Monte Carlo simulations—due to limitations in the PLUS model framework and computational resources. Future research should integrate uncertainty quantification methods to enhance model robustness and credibility.

4.2. Conclusions

(1) Cropland in the YZRB showed a fluctuating but overall increasing trend from 2000 to 2020, primarily driven by the conversion of forest and grassland into cropland. Although some cropland was lost to forest, grassland, and water bodies, the net gain resulted in a dynamic degree of 0.97%, reflecting continued expansion.

(2) The spatial distribution of cropland shifted significantly, with the centroid migrating northwest (2000–2005), southeast (2005–2015), and back northwest (2015–2020). A consistent northwest–southeast pattern was observed, shaped by topography and climate. Changes in the standard deviational ellipse indicated initial concentration and later dispersion of cropland, aligning with the expansion pattern.

(3) Spatiotemporal changes in cropland were jointly driven by natural and socioeconomic factors, as confirmed by robust PLS-SEM model validation ($Q^2 > 0$, AVE > 0.5, GOF > 0.36). Natural factors had a direct positive influence on cropland increase and mediated the impacts of socioeconomic and distance variables, which mainly exerted negative effects.

(4) The PLUS model accurately simulated land use in 2020 and projected divergent outcomes for 2030 under different policy scenarios. Cropland declined most in the Natural Development and Ecological Protection scenarios, remained relatively stable in the Cropland Protection scenario, and experienced significant losses under Urban Development due to rapid urban expansion.

Author Contributions: Writing—original draft, M.H., review and editing, M.H., methodology, M.H., validation, M.H., investigation, M.H., conceptualization, M.H.; methodology, Y.L. (Yanguo Liu), supervision, Y.L. (Yanguo Liu), investigation, Y.L. (Yanguo Liu), data curation Y.L. (Yanguo Liu); methodology, L.T., data curation, L.T., validation, L.T.; funding acquisition J.L., validation, J.L.; supervision, Z.W., investigation, Z.W., methodology, Z.W.; investigation: Y.L. (Yafeng Lu), methodology:

Y.L. (Yafeng Lu); investigation, W.L., validation W.L.; investigation, Q.T., data curation, Q.T. All authors have read and agreed to the published version of the manuscript.

Funding: This research was supported by the Second Tibetan Plateau Scientific Expedition and Research Program (STEP) (Grant No. 2019QZKK0307), the National Key R&D Program of China (Grant No. 2024YFF1307804).

Data Availability Statement: All data sources are mentioned in the manuscript.

Conflicts of Interest: The authors declare no conflict of interest.

References

1. Su, Y.; Qian, K.; Lin, L.; Wang, K.; Guan, T.; Gan, M. Identifying the driving forces of non-grain production expansion in rural China and its implications for policies on cultivated land protection. *Land Use Policy* **2020**, *92*, 104435. [CrossRef]
2. Zhou, Y.; Li, X.; Liu, Y. Cultivated land protection and rational use in China. *Land Use Policy* **2021**, *106*, 105454. [CrossRef]
3. Foley, J.A.; Ramankutty, N.; Brauman, K.A.; Cassidy, E.S.; Gerber, J.S.; Johnston, M.; Mueller, N.D.; O'Connell, C.; Ray, D.K.; West, P.C.; et al. Solutions for a cultivated planet. *Nature* **2011**, *478*, 337–342. [CrossRef] [PubMed]
4. Godfray, H.C.; Beddington, J.R.; Crute, I.R.; Haddad, L.; Lawrence, D.; Muir, J.F.; Pretty, J.; Robinson, S.; Thomas, S.M.; Toulmin, C. Food security: The challenge of feeding 9 billion people. *Science* **2010**, *327*, 812–818. [CrossRef]
5. Prăvălie, R.; Patriche, C.; Borrelli, P.; Panagos, P.; Roșca, B.; Dumitraşcu, M.; Nita, I.-A.; Săvulescu, I.; Birsan, M.-V.; Bandoc, G. Arable lands under the pressure of multiple land degradation processes. A global perspective. *Environ. Res.* **2021**, *194*, 110697. [CrossRef]
6. Zhang, T.; Cheng, C.; Shen, S.; Yang, Y.; Ye, S. Coupled impact of climate change and human activities on farmland loss on the Tibetan Plateau. *Land Use Policy* **2025**, *154*, 107558. [CrossRef]
7. Wang, Y.; Li, X.; Xin, L.; Tan, M. Farmland marginalization and its drivers in mountainous areas of China. *Sci. Total Environ.* **2020**, *719*, 135132. [CrossRef]
8. Wang, A.; Tao, H.; Ding, G.; Zhang, B.; Huang, J.; Wu, Q. Global cropland exposure to extreme compound drought heatwave events under future climate change. *Weather. Clim. Extrem.* **2023**, *40*, 100559. [CrossRef]
9. Cheng, H.; Wang, X.; Chen, D. Research on Spatial–Temporal Variations of Cultivated Land in China Based on GlobeLand30. *Front. Environ. Sci.* **2022**, *10*, 929760. [CrossRef]
10. Li, X.; Zhang, X.; Jin, X. Spatio–temporal characteristics and driving factors of cultivated land change in various agricultural regions of China: A detailed analysis based on County-level data. *Ecol. Indic.* **2024**, *166*, 112485. [CrossRef]
11. Liu, Y.; Liu, S.; Sun, Y.; Wang, F.; Li, M. Driving forces of cultivated land evolution in agro-pastoral areas on the Qinghai-Tibet Plateau based on ecological niche theory. *J. Clean. Prod.* **2021**, *313*, 127899. [CrossRef]
12. Xiao, Y.; Wang, J.; Wang, B.; Fan, B.; Zhou, G. Soil microbial network complexity predicts soil multifunctionality better than soil microbial diversity during grassland–farmland–shrubland conversion on the Qinghai-Tibetan Plateau. *Agric. Ecosyst. Environ.* **2025**, *379*, 109356. [CrossRef]
13. Haddaway, N.R.; Styles, D.; Pullin, A.S. Evidence on the environmental impacts of farm land abandonment in high altitude/mountain regions: A systematic map. *Environ. Evid.* **2014**, *3*, 17. [CrossRef]
14. Zhu, Z.; Qiu, S.; Ye, S. Remote sensing of land change: A multifaceted perspective. *Remote Sens. Environ.* **2022**, *282*, 113266. [CrossRef]
15. Valjarević, A.; Morar, C.; Brasanac-Bosanac, L.; Cirkovic-Mitrovic, T.; Djekic, T.; Mihajlović, M.; Milevski, I.; Culafic, G.; Luković, M.; Niemets, L.; et al. Sustainable land use in Moldova: GIS & remote sensing of forests and crops. *Land Use Policy* **2025**, *152*, 107515. [CrossRef]
16. Lange, S.; Müller, F. Geographic Information Systems (GIS) and Terrestrial Ecosystems. In *Reference Module in Earth Systems and Environmental Sciences*; Elsevier: Amsterdam, The Netherlands, 2024.
17. Duan, X.; Haseeb, M.; Tahir, Z.; Mahmood, S.A.; Tariq, A. Analyzing and predicting land use and land cover dynamics using multispectral high-resolution imagery and hybrid CA-Markov modeling. *Land Use Policy* **2025**, *157*, 107655. [CrossRef]
18. He, Y.; Wu, W.; Xie, X.; Ke, X.; Song, Y.; Zhou, C.; Li, W.; Li, Y.; Jing, R.; Song, P.; et al. Land Use/Cover Change Prediction Based on a New Hybrid Logistic–Multicriteria Evaluation–Cellular Automata–Markov Model Taking Hefei, China as an Example. *Land* **2023**, *12*, 1899. [CrossRef]
19. Luo, G.; Yin, C.; Chen, X.; Xu, W.; Lu, L. Combining system dynamic model and CLUE–S model to improve land use scenario analyses at regional scale: A case study of Sangong watershed in Xinjiang, China. *Ecol. Complex.* **2010**, *7*, 198–207. [CrossRef]
20. Lin, Z.; Peng, S. Comparison of multimodel simulations of land use and land cover change considering integrated constraints—A case study of the Fuxian Lake basin. *Ecol. Indic.* **2022**, *142*, 109254. [CrossRef]

21. Liu, X.; Liang, X.; Li, X.; Xu, X.; Ou, J.; Chen, Y.; Li, S.; Wang, S.; Pei, F. A future land use simulation model (FLUS) for simulating multiple land use scenarios by coupling human and natural effects. *Landsc. Urban Plan.* **2017**, *168*, 94–116. [CrossRef]
22. Zhang, Y.; Yu, P.; Tian, Y.; Chen, H.; Chen, Y. Exploring the impact of integrated spatial function zones on land use dynamics and ecosystem services tradeoffs based on a future land use simulation (FLUS) model. *Ecol. Indic.* **2023**, *150*, 110246. [CrossRef]
23. Zhang, Z.; Hu, B.; Jiang, W.; Qiu, H. Spatial and temporal variation and prediction of ecological carrying capacity based on machine learning and PLUS model. *Ecol. Indic.* **2023**, *154*, 110611. [CrossRef]
24. Zhang, J.; Cao, P.; Roosli, R. Assessing land use and carbon storage changes using PLUS and InVEST models: A multi-scenario simulation in Hohhot. *Environ. Sustain. Indic.* **2025**, *26*, 100655. [CrossRef]
25. Shi, J.; Zhang, P.; Liu, Y.; Tian, L.; Cao, Y.; Guo, Y.; Li, J.; Wang, Y.; Huang, J.; Jin, R.; et al. Study on spatiotemporal changes of wetlands based on PLS-SEM and PLUS model: The case of the Sanjiang Plain. *Ecol. Indic.* **2024**, *169*, 112812. [CrossRef]
26. Wang, C.; Ma, L.; Zhang, Y.; Chen, N.; Wang, W. Spatiotemporal dynamics of wetlands and their driving factors based on PLS-SEM: A case study in Wuhan. *Sci. Total Environ.* **2022**, *806*, 151310. [CrossRef]
27. Li, F.; Xu, Z.; Feng, Y.; Liu, M.; Liu, W. Changes of land cover in the Yarlung Tsangpo River basin from 1985 to 2005. *Environ. Earth Sci.* **2013**, *68*, 181–188. [CrossRef]
28. Huang, X.; Wang, Y.; Wang, X.; Chen, J.; Ma, J.; Liang, E.; Wang, X. Exploring the natural–socioeconomic driving and response mechanisms of ecosystem services interactions to optimize ecosystem management: A case study in the Yarlung Zangbo River Basin. *Sci. Total Environ.* **2024**, *957*, 177842. [CrossRef]
29. Gu, H.; Xu, Y.-P.; Wang, L.; Ma, D.; Liang, X.; Guo, Y.; Liu, L. Seasonal streamflow forecasting by surrogate modeling in the Yarlung Zangbo River Basin, China. *J. Hydrol. Reg. Stud.* **2024**, *53*, 101835. [CrossRef]
30. Li, C.; Hao, J.; Zhang, G.; Fang, H.; Wang, Y.; Lu, H. Runoff variations affected by climate change and human activities in Yarlung Zangbo River, southeastern Tibetan Plateau. *CATENA* **2023**, *230*, 107184. [CrossRef]
31. Li, D.; Chen, G.; Xi, Z.; He, P.; Xin, X.; Chen, J.; Yu, H.; Kang, G. Spatiotemporal changes of cultivated land utilization in black soil region, China based on geo–information Tupu. *Sci. Rep.* **2025**, *15*, 10306. [CrossRef]
32. Yang, G.; Wang, H.; Wang, L.; Shao, W. Analysis of the relationship between food production, water resources and power consumption in North China. *Energy Procedia* **2017**, *142*, 2574–2579. [CrossRef]
33. Guo, N.; Shi, X.; Zhao, Y.; Xu, S.; Wang, M.; Zhang, G.; Wu, J.; Huang, B.; Kong, C. Environmental and Anthropogenic Factors Driving Changes in Paddy Soil Organic Matter: A Case Study in the Middle and Lower Yangtze River Plain of China. *Pedosphere* **2017**, *27*, 926–937. [CrossRef]
34. Shen, W.; Li, H.; Sun, M.; Jiang, J. Dynamics of aeolian sandy land in the Yarlung Zangbo River basin of Tibet, China from 1975 to 2008. *Glob. Planet. Change* **2012**, *86–87*, 37–44. [CrossRef]
35. Zhou, H.; Tang, M.; Huang, J.; Mei, X.; Zhao, H. Driving mechanisms and multi-scenario simulation of land use change based on National Land Survey Data: A case in Jianghan Plain, China. *Front. Environ. Sci.* **2024**, *12*, 1422987. [CrossRef]
36. Wang, X.; Bao, Y. Study on the methods of land use dynamic change research. *Prog. Geogr.* **1999**, *18*, 83–89. [CrossRef]
37. Ye, G.; Chen, K.; Yang, Y.; Liang, S.; Hu, W.; He, L. Integrative Framework for Decoding Spatial and Temporal Drivers of Land Use Change in Malaysia: Strategic Insights for Sustainable Land Management. *Land* **2024**, *13*, 2248. [CrossRef]
38. Grether, J.-M.; Mathys, N. Is the World's Economic Centre of Gravity Already in Asia? *Area* **2010**, *42*, 47–50. [CrossRef]
39. Wang, J.; You, K.; Qi, L.; Ren, H. Gravity center change of carbon emissions in Chinese residential building sector: Differences between urban and rural area. *Energy Rep.* **2022**, *8*, 10644–10656. [CrossRef]
40. Wang, S.; Qin, C.; Zhao, Y.; Zhao, J.; Han, Y. The Evolutionary Path of the Center of Gravity for Water Use, the Population, and the Economy, and Their Decomposed Contributions in China from 1965 to 2019. *Sustainability* **2023**, *15*, 9275. [CrossRef]
41. Chen, P.; Duan, J.; Wang, Y. Spatio–temporal evolution and driving forces of urban gravity centers and ecological security risk gravity centers in China. *Ecol. Indic.* **2025**, *170*, 113025. [CrossRef]
42. Shi, Y.; Matsunaga, T.; Yamaguchi, Y.; Zhao, A.; Li, Z.; Gu, X. Long-term trends and spatial patterns of PM2.5–induced premature mortality in South and Southeast Asia from 1999 to 2014. *Sci. Total Environ.* **2018**, *631–632*, 1504–1514. [CrossRef] [PubMed]
43. Cai, H.; Yu, J.; Guo, Y. Spatial and temporal distribution and evolution of traditional villages in Xin 'an River Basin of China based on geographic detection and remote sensing technology. *Ecol. Indic.* **2025**, *171*, 113239. [CrossRef]
44. Duman, Z.; Mao, X.; Cai, B.; Zhang, Q.; Chen, Y.; Gao, Y.; Guo, Z. Exploring the spatiotemporal pattern evolution of carbon emissions and air pollution in Chinese cities. *J. Environ. Manag.* **2023**, *345*, 118870. [CrossRef]
45. Sander, T.; Teh, P. SmartPLS for the Human Resources Field To Evaluate a Model. In *New Challenges of Economic and Business Development*; University of Latvia: Riga, Latvia, 2014.
46. Sarstedt, M.; Cheah, J.-H. Partial least squares structural equation modeling using SmartPLS: A software review. *J. Mark. Anal.* **2019**, *7*, 196–202. [CrossRef]
47. Liu, C.; Zhang, F.; Jim, C.-Y.; Johnson, V.C.; Tan, M.L.; Shi, J.; Lin, X. Controlled and driving mechanism of the SPM variation of shallow Brackish Lakes in arid regions. *Sci. Total Environ.* **2023**, *878*, 163127. [CrossRef] [PubMed]

48. Liang, X.; Guan, Q.; Clarke, K.C.; Liu, S.; Wang, B.; Yao, Y. Understanding the drivers of sustainable land expansion using a patch-generating land use simulation (PLUS) model: A case study in Wuhan, China. *Comput. Environ. Urban Syst.* **2021**, *85*, 101569. [CrossRef]
49. Guo, A.; Zhang, Y.; Hao, Q. Monitoring and Simulation of Dynamic Spatiotemporal Land Use/Cover Changes. *Complexity* **2020**, *2020*, 3547323. [CrossRef]
50. Wang, Q.; Bai, X.; Zhang, D.; Wang, H. Spatiotemporal characteristics and multi-scenario simulation of land use change and ecological security in the mountainous areas: Implications for supporting sustainable land management and ecological planning. *Sustain. Futures* **2024**, *8*, 100286. [CrossRef]
51. Wang, Z.; Li, Z.; Liu, X.; Song, H.; Liu, S.; Qi, J.; Jing, F.; Gao, Z. Ecological analysis and multi-scenario simulation of Yellow River Delta wetland under clearing of Spartina alterniflora. *Glob. Ecol. Conserv.* **2024**, *56*, e03287. [CrossRef]
52. Wu, Q.; Wang, L.; Wang, T.; Ruan, Z.; Du, P. Spatial–temporal evolution analysis of multi-scenario land use and carbon storage based on PLUS–InVEST model: A case study in Dalian, China. *Ecol. Indic.* **2024**, *166*, 112448. [CrossRef]
53. Li, W.; Kang, J.; Wang, Y. Identifying the contribution and spatial effects of land use conversion on ecosystem health in Chongqing: A multi-scenario simulation perspective. *Ecol. Indic.* **2024**, *165*, 112232. [CrossRef]
54. Xu, C.; Zhang, Q.; Yu, Q.; Wang, J.; Wang, F.; Qiu, S.; Ai, M.; Zhao, J. Effects of land use/cover change on carbon storage between 2000 and 2040 in the Yellow River Basin, China. *Ecol. Indic.* **2023**, *151*, 110345. [CrossRef]
55. Liu, J.; Liu, B.; Wu, L.; Miao, H.; Liu, J.; Jiang, K.; Ding, H.; Gao, W.; Liu, T. Prediction of land use for the next 30 years using the PLUS model's multi-scenario simulation in Guizhou Province, China. *Sci. Rep.* **2024**, *14*, 13143. [CrossRef]
56. Zhang, C.; Jia, Q.; Liu, Y.; Zheng, Z.; Gao, Y.; Li, K. Evaluation and multi scenario simulation of ecosystem service value in Zhengzhou Metropolitan Area based on PLUS model. *Meas. Sens.* **2024**, *32*, 101079. [CrossRef]
57. Lin, X.; Fu, H. Multi-scenario simulation analysis of cultivated land based on PLUS model—A case study of Haikou, China. *Front. Ecol. Evol.* **2023**, *11*, 1197419. [CrossRef]
58. Xu, B.; Li, J.; Liu, Y.; Zhang, T.; Luo, Z.; Pei, X. Disentangling the response of vegetation dynamics to natural and anthropogenic drivers over the Qinghai-Tibet Plateau using dimensionality reduction and structural equation model. *For. Ecol. Manag.* **2024**, *554*, 121677. [CrossRef]
59. Gu, Z.; Chen, X.; Ruan, W.; Zheng, M.; Gen, K.; Li, X.; Deng, H.; Chen, Y.; Liu, M. Quantifying the direct and indirect effects of terrain, climate and human activity on the spatial pattern of kNDVI–based vegetation growth: A case study from the Minjiang River Basin, Southeast China. *Ecol. Inform.* **2024**, *80*, 102493. [CrossRef]
60. Li, C.; Yang, M.; Li, Z.; Wang, B. How Will Rwandan Land Use/Land Cover Change under High Population Pressure and Changing Climate? *Appl. Sci.* **2021**, *11*, 5376. [CrossRef]
61. Liu, Y.; Jing, Y.; Han, S. Multi-scenario simulation of land use/land cover change and water yield evaluation coupled with the GMOP–PLUS–InVEST model: A case study of the Nansi Lake Basin in China. *Ecol. Indic.* **2023**, *155*, 110926. [CrossRef]
62. Zhai, H.; Lv, C.; Liu, W.; Yang, C.; Fan, D.; Wang, Z.; Guan, Q. Understanding Spatio–Temporal Patterns of Land Use/Land Cover Change under Urbanization in Wuhan, China, 2000–2019. *Remote Sens.* **2021**, *13*, 3331. [CrossRef]
63. Zhang, J.; Wang, J.; Chen, Y.; Huang, S.; Liang, B. Spatiotemporal variation and prediction of NPP in Beijing–Tianjin–Hebei region by coupling PLUS and CASA models. *Ecol. Inform.* **2024**, *81*, 102620. [CrossRef]
64. Chen, L.; Cai, H. Study on land use conflict identification and territorial spatial zoning control in Rao River Basin, Jiangxi Province, China. *Ecol. Indic.* **2022**, *145*, 109594. [CrossRef]
65. Demessie, S.F.; Dile, Y.T.; Bedadi, B.; Tarkegn, T.G.; Bayabil, H.K.; Sintayehu, D.W. Assessing and projecting land use land cover changes using machine learning models in the Guder watershed, Ethiopia. *Environ. Chall.* **2025**, *18*, 101074. [CrossRef]
66. Zeng, J.; Luo, T.; Gu, T.; Chen, W. How does cultivated land fragmentation affect soil erosion: Evidence from the Yangtze River Basin in China. *J. Environ. Manag.* **2024**, *360*, 121020. [CrossRef]
67. Huang, X.; Wang, H.; Xiao, F. Simulating urban growth affected by national and regional land use policies: Case study from Wuhan, China. *Land Use Policy* **2022**, *112*, 105850. [CrossRef]
68. Wei, Q.; Abudureheman, M.; Halike, A.; Yao, K.; Yao, L.; Tang, H.; Tuheti, B. Temporal and spatial variation analysis of habitat quality on the PLUS–InVEST model for Ebinur Lake Basin, China. *Ecol. Indic.* **2022**, *145*, 109632. [CrossRef]
69. Wu, J.; Luo, J.; Zhang, H.; Qin, S.; Yu, M. Projections of land use change and habitat quality assessment by coupling climate change and development patterns. *Sci. Total Environ.* **2022**, *847*, 157491. [CrossRef]
70. Loukika, K.N.; Keesara, V.R.; Buri, E.S.; Sridhar, V.; Dzwairo, B.; Montenegro, S. Integrated impacts of land use changes and climate dynamics on hydrological components in the Munneru River basin, India. *J. Environ. Manag.* **2025**, *380*, 125096. [CrossRef]
71. Wang, X.; Wang, D.; Wu, S.; Yan, Z.; Han, J. Cultivated land multifunctionality in undeveloped peri–urban agriculture areas in China: Implications for sustainable land management. *J. Environ. Manag.* **2023**, *325*, 116500. [CrossRef]
72. Li, S.; Pu, J.; Deng, X. Agricultural land use transition under multidimensional topographical gradients and its impact on ecosystem service interactions. *J. Integr. Agric.* **2025**, *in press*.

73. Tarolli, P.; Straffelini, E. Agriculture in Hilly and Mountainous Landscapes: Threats, Monitoring and Sustainable Management. *Geogr. Sustain.* **2020**, *1*, 70–76. [CrossRef]
74. Seydehmet, J.; Zhou, X.; Chen, H.; Wang, Y. The spatiotemporal evaluation of ecosystem stability by simulating land use change in edge oasis of the Tarim basin, northwest China. *Heliyon* **2025**, e42621. [CrossRef]
75. Bren d'Amour, C.; Reitsma, F.; Baiocchi, G.; Barthel, S.; Güneralp, B.; Erb, K.H.; Haberl, H.; Creutzig, F.; Seto, K.C. Future urban land expansion and implications for global croplands. *Proc. Natl. Acad. Sci. USA* **2017**, *114*, 8939–8944. [CrossRef]
76. Ibraeva, A.; Correia, G.H.d.A.; Silva, C.; Antunes, A.P. Transit–oriented development: A review of research achievements and challenges. *Transp. Res. Part A Policy Pract.* **2020**, *132*, 110–130. [CrossRef]
77. Tong, X.; Wang, Y.; Chan, E.H.W.; Zhou, Q. Correlation between Transit–Oriented Development (TOD), Land Use Catchment Areas, and Local Environmental Transformation. *Sustainability* **2018**, *10*, 4622. [CrossRef]
78. Zhou, J.; Johnson, V.C.; Shi, J.; Tan, M.L.; Zhang, F. Multi-scenario land use change simulation and spatial–temporal evolution of carbon storage in the Yangtze River Delta region based on the PLUS–InVEST model. *PLoS ONE* **2025**, *20*, e0316255. [CrossRef]
79. Shi, X.; Wang, W.; Shi, W. Progress on quantitative assessment of the impacts of climate change and human activities on cropland change. *J. Geogr. Sci.* **2016**, *26*, 339–354. [CrossRef]

Disclaimer/Publisher's Note: The statements, opinions and data contained in all publications are solely those of the individual author(s) and contributor(s) and not of MDPI and/or the editor(s). MDPI and/or the editor(s) disclaim responsibility for any injury to people or property resulting from any ideas, methods, instructions or products referred to in the content.